CEEGS DELIVERABLE D2.1

Geological scenarios and their characteristics

Summary:

In this WP2 deliverable, possible geological scenarios and the limitations they impose to the CEEGS concept are addressed. Analytical solutions are used to study the key issues of initial plume setp in a porous media and the reservoir depth restrictions imposed by pressure losses in wellbores. The same analytical solutions, using a Monte Carlo approach, allow to study the sensitivity of the P-T conditions expected at the CO_2 injection and back-production wells. The scenarios considered cover porous media (deep saline aquifers or depleted hydrocarbon fields and salt cavities) with different configurations and characterised by ranges of hydraulic and thermodynamic conditions.

Authors:

Júlio Carneiro, Converge!, Lda

Dounya Behnous, Converge!, Lda

Funded by the European Union

Title:	Geological scenarios and their characteristics.
Lead beneficiary:	CONV
Other beneficiaries:	Other PP involved in the preparation of the deliverable
Due date:	6th month (April)
Nature:	Public
Diffusion:	e.g. all Partners, WP-partners
Status:	Live document
DOI:	
License information:	
Recommended Citation:	Carneiro, J. and Behnous, B. (2023) - Geological scenarios and their characteristics. Deliverable D2.1 CEEGS. Évora, 50 pp.
Related Data:	
ORCID:	Carneiro, J.: 0000-0002-4900-3355
Document code:	CEEGS_D.2.1

Revision history	Author	Delivery date	Summary of changes and comments
Version 01	NN	28/04/2023	First version
Version 02	NN	XX.XX.XXXX	
Final version	NN	XX.XX.XXXX	

Approval status				
	Name	Function	Date	Signature
Deliverable responsible	Júlio Carneiro		28/04/2023	
WP leader	Júlio Carneiro		28/04/2023	
Reviewer				
Reviewer				
Project Coordinator				

Funded by the European Union. Views and opinions expressed are however those of the author(s) only and do not necessarily reflect those of the European Union or CINEA. Neither the European Union nor the granting authority can be held responsible for them.

TABLE OF CONTENTS

FIGURES

TABLES

1 EXECUTIVE SUMMARY

The overall objective of WP2 is to define the geological scenarios in which the CEEGS technology can effectively store energy and promote CO_2 sequestration in the subsurface. In task 2.1, to which this deliverable refers, an implementation of analytical and semi-analytical solutions for CO_2 flow and thermodynamic behavior in wellbores and geological reservoirs has been carried out. Those solutions allow to analyze the constraints that reservoir depth, petrophysical parameters and hydraulic conditions may impose to the implementation of the CEEGS concept in these environments. This approach was applied to: i) porous media, either deep saline aquifers or depleted hydrocarbon fields; ii) salt cavities. The overall goal of the deliverable is to provide a first identification of the likely scenarios in which the CEEGS concept can potentially be applied and the constraints imposed by those geological environments to its implementation.

The study encompassed both open and porous media reservoirs, and included the possibility of simultaneous utilization of two porous media reservoirs at different depths. It is recommended that site selection for porous media reservoirs, put less weigth on finding high permeability-high porosity, very thick reservoirs (type I reservoirs) ,as is often the case in the CO_2 storage technology, and is suggested that lower quality (type II and III) thinner reservoirs may present more favourable conditions for CEEGS. It is also recommended that the minimum reservoir depth to be deeper than in the CO_2 storage industry, at least 1300 m, to avoid CO_2 in-well phase transition.

Salt cavities scenarios were addressed for scenarios involving a single cavity coupled with surface CO_2 storage in a tank, but also in two salt cavities at different depths (or managed at different pressures). The range of admissible depths for the cavities and the expected wellhead pressures that can be obtained were studied for simplified cases.

The deliverable concludes by listing the realistic geological scenarios that should be studied using numerical models in subsequent tasks of WP2, and if proved valid, in other WPs. The scenarios include various configurations of deep saline aquifers (open structure, closed structure, two aquifers), depleted hydrocarbon fields (closed structure), geothermal sedimentary system, and salt cavities (one single cavity with surface storage of CO_2, and two salt cavities). The numerical modelling studies will address the transient behaviour of the reservoirs, to understand the cyclic and long term evolution of pressure and temperature in the reservoir and wellheads, and chemical changes that may occur during the injection and back-prodution cycles due to the interaction between the CO_2 and the brine and mineral components of the reservoir.

2 INTRODUCTION

The CEEGS concept aims to integrate an electrothermal and geological storage energy storage system, based on renewable energy, in which the CO_2 captured in a power plant or industrial facility is used as a working fluid in a heat pump for storing surplus renewable energy in the thermal (at surface) and mechanical (underground) forms. The inevitable CO_2 fluid losses in the underground are seen as an added benefit of the CEEGS technology, since it allows for long term CO_2 sequestration. Since the geological reservoir needs to be at considerable depth, a small geothermal heat gain may occur, adding to the energy that can be recovered through the expansion of CO_2 in a turbine.

Figure 1: shows a conceptual scheme of the CCEGS concept, consisting of two independent and open CO_2 cycles, connected directly by geological storage and indirectly by thermal storage. CO_2 captured in a stationary source is used as a working fluid in a heat pump and injected into a geological formation (sequence 0-4-1-2-3-A), performing a charging cycle equivalent to that of the electrothermal system in the high (HT) and low (LT) temperature reservoirs. For the discharge, CO_2 is extracted from the geological formation and used as the working fluid in the reverse cycle, ending with the re-injection of CO_2 into the geological formation (sequence A-6-7-8-5-B).

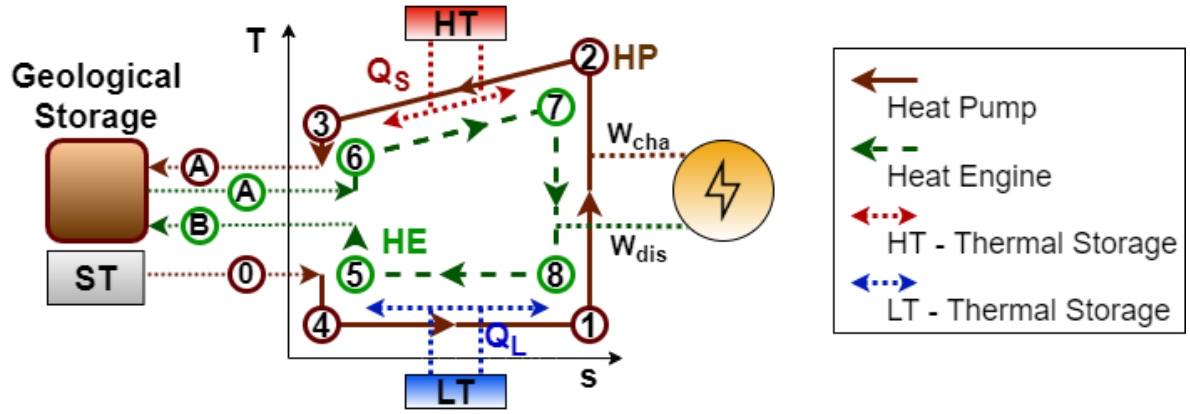

Figure 1: Schematic representation of the CEEGS concept. Q_S: Sensible Heat; Q_L: Latent Heat; W: Work; cha: Charge; dis: Discharge; ST: Stationary CO_2 source.

The geological storage component implies three operational stages:

i. Setup stage - in which CO_2 is continuously injected in one or several wells for a period of time and at a mass flow rate enough to ensure the development of a large CO_2 plume in supercritical phase. The CO_2 plume will cause the lateral migration of the formation water away from the injection wells and minimise the risk of water production during the subsequent stages. This stage occurs only at the onset of the energy storage system;
ii. Charge stage - in which renewable electricity in excess is transformed into thermal energy (stored at surface) and into mechanical energy through injection of the CO_2, via one or more wells, in the supercritial plume created in the setup stage;
iii. Discharge stage - in which supercritical CO_2 is produced in one or more wells, runs through a heat engine and a turbine to restore energy and is reinjected underground in a different set of wells in liquid phase;

The charge and the discharge stages run alternating during the lifetime of the system, not necessarily in immediate continuity, as they may be separated by a period without injection or production of CO_2. The duration of the charge and discharge stages does not have to be the same and can last from hours to a seasonal time scale (to be studied in WP4). For the sake of the analysis in this deliverable, the duration of the charge and discharge stages is in the order of hours.

The CO_2 injection process is a matured technology, being employed by the oil industry since 1972. Currently, and worldwide, the mass of annually injected CO_2 is above 40 Mt of CO_2 for enhanced hydrocarbon recovery (EOR) purposes or for CO_2 capture and storage (CCS) as a climate mitigation technology.

The selection of geological reservoirs for CCS purposes is well established and documented (e.g. Bachu, 2003; Bachu (2008); Metz et al., 2005; NETL, 2013; Oldenburg, 2008) and applies to CEEGS, including the need to ensure not only a suitable porous and permeable reservoir but also a very low permeability cap-rock that prevents CO_2 from ascending to the surface by buoyancy.

In CCS, the shape and spread of the plumes are of concern for safety reasons. CEEGS faces different challenges**. The free-phase CO_2 plume extent must be understood in advance for the position of the wells to ensure the minimal withdrawal of formation water (brine) together with the back-produced supercritical CO_2.** The extent and shape of the plume will be a function of the heterogeneity, geometry of the reservoir, and its petrophysical and hydraulic properties. Still, identifying the reservoirs' characteristics that favour the early development of a large enough plume is relevant to understand the constraints imposed by the geological environments to the CEEGS technology.

Moreover, the efficiency of the CEEGS with CO_2 underground injection and back-production depends mainly on pressure (P) and temperature (T) conditions at the reservoir and P-T variation between wellheads and bottomholes**. These are primarily a function of the flow rates and well diameters, but also of length of the wells, i.e. of reservoir depths.** The P-T changes within the well are particularly relevant for the back-production of CO_2 from the reservoir, in order to ensure that the CO_2 saturation line is not reached and two-phase flow does not occur in the producing well.

Task 2.1, and this deliverable, rely on the implementation of analytical and semi-analytical solutions for CO_2 flow and thermodynamic behavior in the wells and in the reservoir to analyse constraints that reservoir depth, petrophysical parameters and hydraulic conditions may impose to the implementation of the CEEGS concept in different geological environments. This approach was applied to: i) **porous media**, either deep saline aquifers or depleted hydrocarbon fields; ii) **salt cavities**.

This report is organised as follows: chapter 2 describes the methods applied, namely the analytical and semi-analytical solutions; chapters 3 and 4 describe the results obtained with those solutions for porous media scenarios and salt cavity scenarios, respectively. Chapter 5 summarises the main features of the scenarios to be implemented numerically in subsequent tasks and WPs. Chapter 6 presents the conclusions of the report. This deliverable is complemented by a set of excel datafiles with the results of the scenarios described in chapters 3 and 4.

3 METHODS

This chapter presents the analytical and semi-analytical solutions for CO_2 flow in the well and in the geological reservoir implemented. The following solutions are described:

i) an analytical solution for the CO_2 / brine interface in a porous media;
ii) A second analytical model allows the calculation of the pressure build-up during the injection of CO_2 in a porous media;
iii) a wellbore flow model evaluates the P-T changes between the wellhead and the bottomhole due to the ascending/descending CO_2;
iv) A thermodynamic model is used to study P-T changes in a salt cavity in which CO_2 is stored.

3.1 ANALYTICAL SOLUTION FOR CO_2-BRINE INTERFACE IN A POROUS MEDIA

Many authors have investigated the CO_2/brine interface dynamic during CO_2 injection into porous media, usually in the scope of CCS studies (e.g. Pruess and Garc, 2002, Riaz et al., 2006, Nordbotten and Celia, 2006). Nordbotten and Celia (2006) used an approach derived from the Buckley and Leverett equation (Buckley and Leverett, 1941) to evaluate the pressure buildup for immiscible flow during the injection of supercritical CO_2 into a porous formation. The major advantage of this model is that the saturation distribution can be derived explicitly. Dentz and Tartakovsky (2009) developed an approximate analytical solution describing the dynamics of interface in two and three-dimensional porous media, by providing a general approach and incorporating the buoyancy effects which rely on the Dupuit approximation. This approach is applicable to a variety of situations involving variable-density flows in porous media.

In Nordbotten and Celia (2006) the reservoir is considered as a confined, uniform and homogeneous porous media. The model retrieves a sharp CO_2 / brine interface, with the thickness of the lighter fluid (CO_2) denoted by h (r, t) lying above the denser brine (Figure 2). The main assumptions of this model are that fluids and porous formations are considered incompressible, and viscosity and relative permeability are assumed constant within each zone.

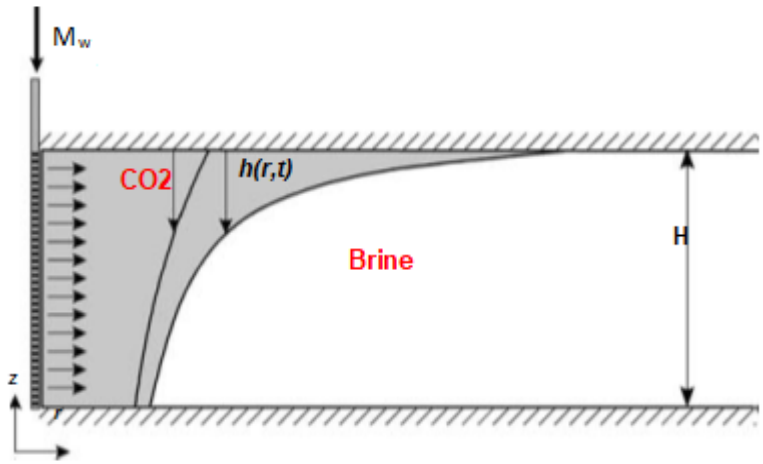

Figure 2: Schematic diagram showing the interface of thickness h(r,t) adapted from (Nordbotten and Celia, 2006).

Considering a fully penetrating well centered at r = 0 with a finite radius r_w and a constant mass flowrate M_w, the model establishes how the interface between the two fluids (CO_2 and brine) will respond at different reservoir and flow rate conditions, according to equation 1.

$$h_D = \begin{cases} 0 & x \le 2\gamma & \text{CO2 only} \\ \frac{\{2\gamma/x\}^{1/2}-1}{\gamma-1} & 2\gamma < x < \frac{2}{\gamma} & 2-\text{phase region} \\ 1, & x \ge \frac{2}{\gamma} & \text{brine region} \end{cases} \quad (1)$$

considering the following dimensionless groups:

$$t_D = \frac{M_w t}{2\pi \emptyset H \rho_0 r_w^2}; P_D = \frac{2\pi H \rho_0 kp}{M_w \mu_0}; x = \frac{r_D^2}{t_D}; r_D = \frac{r}{r_w}; h_D = \frac{h}{H}; \alpha = \frac{M_w \mu_{0(C_r+C_w)}}{2\pi H \rho_0 k}; \beta = \frac{M_w kb}{2\pi H r_w \mu_o};$$

$$\gamma = \frac{\mu_o}{\mu_w};$$

where t: time, Ø: porosity, r: radial distance from the injection well (m); H: formation thickness (m), b: Forchheimer parameter, r_w: well radius (m), M_W: mass flow rate (kg/s), k: permeability (md), c_r: rock compressibility (Pa^{-1}), c_w: water compressibility (Pa^{-1}), μ_w: viscosity of brine (Pa^{-1}), μ_0: viscosity of CO_2. P: Brine density (kg/m^3). A: compressibility parameter, β: inertial parameter, and γ: viscosity ratio, are three dimensionless parameters, *while* P_D is dimensionless pressure.

3.2 ANALYTICAL SOLUTION FOR PRESSURE BUILD-UP IN A POROUS MEDIA

Mathias et al., (2009) improved Nordbotten and Celia, (2006) approach and developed analytical solutions to estimate the pressure build-up due to CO_2 injection in a deep saline aquifer by using matched asymptotic expansions. The study was carried out on a formation with an infinite radial extent. Later, the solution was extended to account for finite outer boundaries by invoking a quasi-static condition (Mathias et al., 2011) and verified by comparison with vertically averaged results from TOUGH2 simulations of the fully dynamic problem (Figure 3).

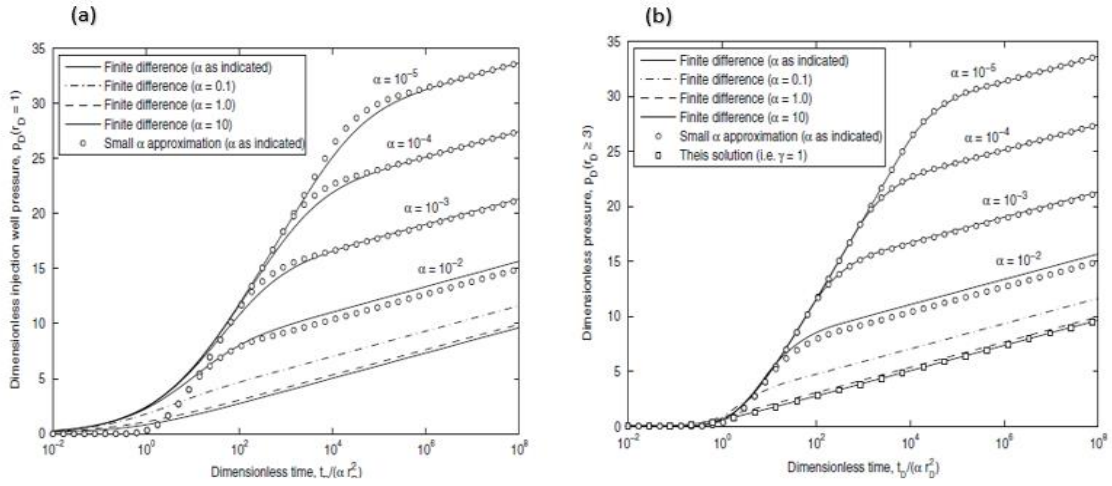

Figure 3 : Validation of the Mathias et al. (2009) solution against numerical simulations with TOUGH2. Dimensionless pressure, p_D, against $t_D/(\alpha r_D^2)$ at the well boundary (a) for (r_D = 1), (b) for ($r_D \ge 3$) (Mathias et al., 2009)

Mathias et al. (2009) pressure buildup model, applicable to open structures (i.e., without lateral impermeable barriers that can prevent brine migration), using the same notation as in equation 1, is given by:

$$P_D = \begin{cases} -\frac{1}{2} ln\left(\frac{x}{2\gamma}\right) - 1 + \frac{1}{\gamma} - \frac{1}{2\gamma}\left[ln\left(\frac{\alpha}{2\gamma^2}\right) + 0.5772\right] & x \le 2\gamma \\ -\left(\frac{x}{2\gamma}\right)^{\frac{1}{2}} + \frac{1}{\gamma} - \frac{1}{2\gamma}\left[ln\left(\frac{\alpha}{2\gamma^2}\right) + 0.5772\right] & 2\gamma < x < 2/\gamma \\ -\frac{1}{2\gamma}\left[ln\left(\frac{\alpha x}{4\gamma}\right) + 0.5772\right] & x \ge 2/\gamma \end{cases} \quad (2)$$

A simplified approach by Bergmo et al. (2011) was utilized os closed structures (i.e, with lateral impermeable boundaries), according to which the overpressure (DP) induced by a volume of injected CO_2 (V_c) is given by:

$$\Delta P = \frac{V_c}{V_{por}(c_r + \emptyset c_w)} \quad (3)$$

The pressure increment ΔP occurring in a given time period was added to the solution provided by Mathias et al. (2009) as an approximation for the pressure build-up in a closed structure. Rock compressibilities were computed following Yale et al. (1993) solution, taking into account reservoir depth and pressure for a consolidated sandstone reservoir.

3.3 ANALYTICAL WELLBORE FLOW MODEL

To simulate the flow in the injection and production wells a sufficiently large CO_2 plume is assumed to be established in the reservoir before the discharge stage, to avoid brine production. Pruess (2006) performed a detailed numerical reservoir simulations of the classic five well spots pattern comparing CO_2 with water, assuming realistic thermophysical parameters. In his study, the physics of heat and fluid in the wells was simplified by considering isenthalpic transformation and gravitationally static conditions to produce an estimated wellhead condition.

Atrens et al., (2009) considered wells under purely static gravitational conditions, and their models were later refined in Atrens et al., (2010) to include frictional effects, concluding that they were significant. In their model the temperature variation in the reservoir between the injection and production wells follows a linear temperature gradient. Pan et al., (2015) used T2Well-ECO2N, a fully coupled wellbore-reservoir simulator (Pan et al., 2011, Pan and Oldenburg, 2013), in which the wellbore-reservoir flow problem is treated as an integrated system and the flow is controlled by different physics for the two subdomains.

In this study, we chose to apply the wellbore model of Adams et al. (2014). This model is employed to calculate the P-T differences between the wellhead and the bottomhole due to the flow of injected/back-produced CO_2. In Adams et al. (2014) by subdividing the well into (*n*) segments, the energy balance, the momentum balance, and the continuity equation are solved for the fluid state at (*i*+1) using the initial (previous) state (*i*) as shown in equations 4 to 6.

$$\begin{cases} h_i + \frac{v_i^2}{2} + gz_i = h_{i+1} + \frac{v_{i+1}^2}{2} + gz_i & (4) \\ P_i + \frac{\rho_i v_i^2}{2} + \rho_i g z_i = P_{i+1} + \frac{\rho_{i+1} v_{i+1}^2}{2} + gz_{i+1} & (5) \\ \dot{m} = \rho_i A v_i = \rho_{i+1} A v_{i+1} & (6) \\ \Delta P = f \frac{L_{pipe}}{D} \frac{\rho v^2}{2} = f \frac{L_{pipe}}{D^5} \frac{8\dot{m}}{\rho \pi^2} & (7) \end{cases}$$

where f: friction factor, D: well diameter (m), V: fluid velocity(m/s), L: length of the well (m), $\dot{m}$: mass flowrate (kg/s), A: cross sectional area (m^2), P: pressure (MPa). h: specific enthalpy (Kj/kg), ρ: density(kg/m^3).

The friction losses are determined from the Darcy-Weisbach relation, (equation 7). In this report, a constant friction factor for the wellbore materials was used as 0.1.

To calculate the changes in P, T and enthalpy as the CO_2 flows in the wellbore, the TOUGH2/ECO$_2$N tables for density, viscosity, and specific enthalpy of pure CO_2 were applied on a regular grid of (T, P) values (Pruess, 2005).

3.4 ANALYTICAL THERMODYNAMIC MODEL FOR SALT CAVITIES

The majority of studies modelling storage of gases in salt cavities are mainly related to two different problems. The first one focuses on the mechanical behavior of the salt cavity, thus modelling the viscoelastic behavior of the rock salt, analyses the stability criterion and long term integrity of the cavern (Hou, 2003, Minkley and Mühlbauer, 2017, Khaledi et al., 2016, Zhang et al., 2017, Cornet et al., 2018). The other group of studies focused on the thermodynamic behavior of the stored gas inside the salt cavern, where the objective is to anticipate the evolution of the gas conditions under various injection and withdrawal operations and the heat exchanges with the rock mass (Kushnir.R et al., 2012, Raju and Khaitan, 2012, Xia et al., 2015, Alvarez et al., 2022). Other studies focus in coupling the thermodynamic behaviour of the gas to the thermomechanical behaviour of the solid (Khaledi et al., 2016, Pola, 2021).

CEEGS is interested on the thermodynamical aspect, on the evaluation of pressure and temperature variation inside the cavern during injection and withdrawal process, and its impact on the wellhead pressures and temperature. As suggested in Kushnir et al., (2012), Raju and Khaitan (2012), Xia et al. (2015), the volume change of the cavern itself is considered small, so its effect of CO_2 pressure and temperature is neglected. That is, the cavern volume is assumed to be constant.

The model employed to evaluate the pressure and temperature variation resulted from the CO_2 charge and discharge processes from the salt cavity is described using an analytical thermodynamic model as presented by Khaledi et al. (2016). By combining the mass and energy equation, the following ordinary differential equation is obtained and used to describe the CO_2 variation inside the salt cavity:

$$\rho_a (C_a - R)\dot{T}_a + \frac{\dot{m_{in}} c_a}{V}(T_a - T_{in}) + \frac{RT_a}{V}(\dot{m_{out}} - \dot{m_{in}}) + \frac{h_c A_c}{V}(T_a - T_s) \qquad (8)$$

where, h_c is the heat transfer coefficient between the cavern wall and the CO_2 and A_c is the heat transfer area. T_a and T_s represent the temperature of CO_2 inside the cavern and the surrounding rock. $\dot{m_{out}}$ and $\dot{m_{in}}$ denote the mass flow rate over the discharge and charge time, respectively (Figure 4).

Having CO_2 properties at the inlet and outlet of the cavern (i.e. at the bottomhole), the equation above is solved for any time *t*, resorting to an implicit finite difference scheme isconsidering the minimum and maximum depth and pressure allowed in salt cavities. The heat transfer between the cavern wall and CO2 (the last term in equation 8) is not considered because heat transfer is assumed to be negligible for the short-term charge / discharge cycles addressed in this report.

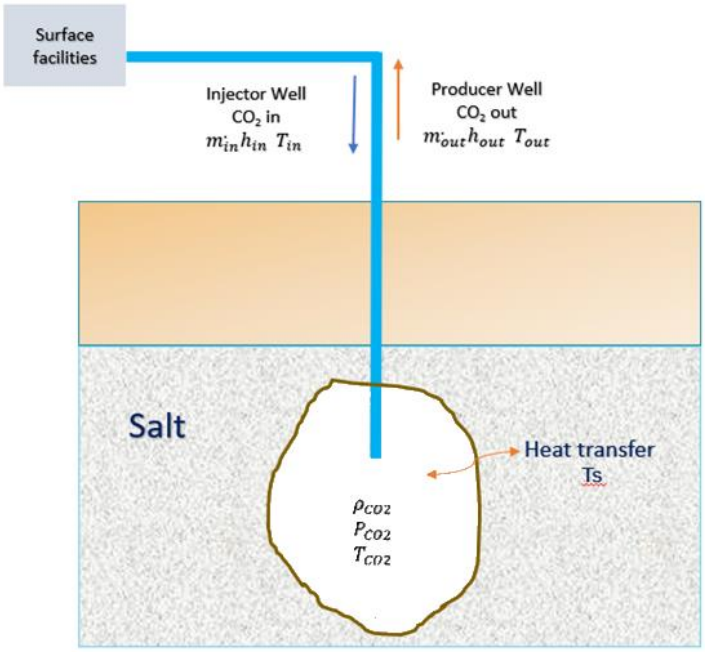

Figure 4: Schematic diagram of control volume and CO_2 properties at the inlet and outlet during the charge and discharge processes from rock salt cavity (adapted from Khaledi et al., 2016)**.**

3.5 IMPLEMENTATION OF THE ANALYTICAL SOLUTIONS

Since the objective of task 2.1 is to identify the constraints imposed by certain geological environments and to understand the sensitivity of the plume size and of P-T changes at the wellhead (i.e., the connection to the surface components), *@RISK* excel add-in was used to implement multiple realisations through a Monte Carlo procedure in spreadsheets in which the analytical solutions described above were coded in VBA. The pressure build-up model for porous media and the thermodynamic model for the salt cavity were coupled with the wellbore flow model through the bottomhole pressure, allowing for a pressure discrepancy between the reservoir pressure and the bottomhole pressure to account for a "skin" effect in the wellbore. The pressure build-up was limited to 20% of the initial reservoir pressure (always considered at hydrostatic conditions) to avoid the risk of fracturing the reservoir or seal.

4 POROUS MEDIA SCENARIOS

Different geological environments and scenarios can be considered for implementing the subsurface component of the technology. Based on a literature review for technologies that show common features with CEEGS (such as CCS, CO_2 -Enhanced Geothermal Ssystems, and Compressed Air Energy Storage - CAES), the geological environments and scenarios to be considered in subsequent tasks of WP2 and, if proved valid in other work packages, include the porous media reservoir, either deep saline aquifers or depleted hydrocarbon fields, and salt cavities. This chapter discusses the porous media scenarios.

4.1 SETUP STAGE IN POROUS MEDIA RESERVOIR

In the CEEGS concept, the initial setup of the energy storage system implies the injection of a large volume of CO_2 in a porous media reservoir that will displace the brine and develop a supercritical CO_2 plume. The size of the free-phase plume obviously depends on the injection mass flowrate and injection time, but also on reservoir properties, namely on reservoir depth, porosity permeability, thickness, rock compressibility, and on well radius and geothermal gradient.

Equation 1 shows the relation between those parameters and the plume size, but in order to understand the sensitivity to the different parameters, the interface height h(r,t) solution given by Nordbotten and Celia (2006) was implemented in *@Risk* Monte Carlo and simulations were conducted for a range of realistic reservoir and rock parameters. The Nordbotten and Celia (2006) solution allows to calculate the radial extent of the plume from the base to the top of the reservoir, but task 2.1 analysed the plume radial extent at three vertical locations within the reservoir, namely, at the base *h(r, t)=0*, at the middle *h(r,t)=H/2*, and at the top *h(r,t)=H* of the reservoir (Figure 5).

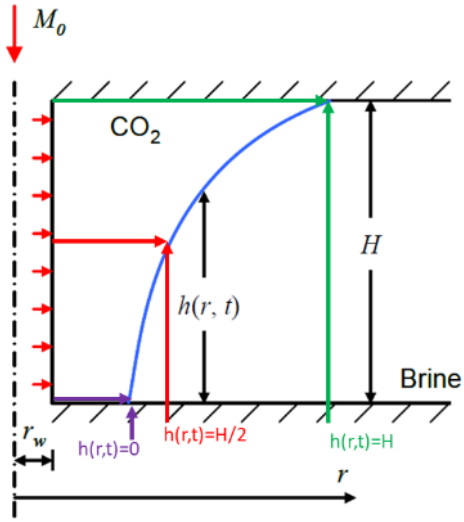

Figure 5: Representation of base extent, middle extent and top extent of the plume

Monte Carlo simulations were performed using 200 000 realisations from a range of values listed in Table 1. Time of injection was kept constant at 100 days and mass flow rate at 100kg/s.

Figure 6 illustrates the plume size (or in fact, the base, middle and top extent of the plume) with respect to porosity, thickness, permeability and depth, for a well diameter of 0.5m, with all other parameters remaining constant for each of the cases illustrated in Figure 6. As expected from equation 1, in these specific cases, results show that smaller porosities and thicknesses provide a thicker plume.

Table 1: Range of values considered for initial plume setup analysis

Parameter	Range of values				
Depth (m)	800	1500	2000	2500	3000
CO_2 mass rate (kg/s)	1	10	50	100	
Well diameter (m)	0.20	0.3	0.4		
Geothermal gradient (°C /km)	20	30	40		
Intrinsic permeability (k)	5.00E-14	1.00E-13	5.00E-13	1.00E-12	
Reservoir thickness (H)	50	100	200		
Porosity (ϕ)	0.03	0.1	0.2	0.3	
Reservoir Pressure (MPa	As function of depth. Hydrostatic pressure using a brine salinity value of 1025 kg/m^3.				
Reservoir temperature (°C)	As function of depth and geothermal gradient. Estimated considering a uniform geothermal gradient and constant surface temperature of 15°C.				

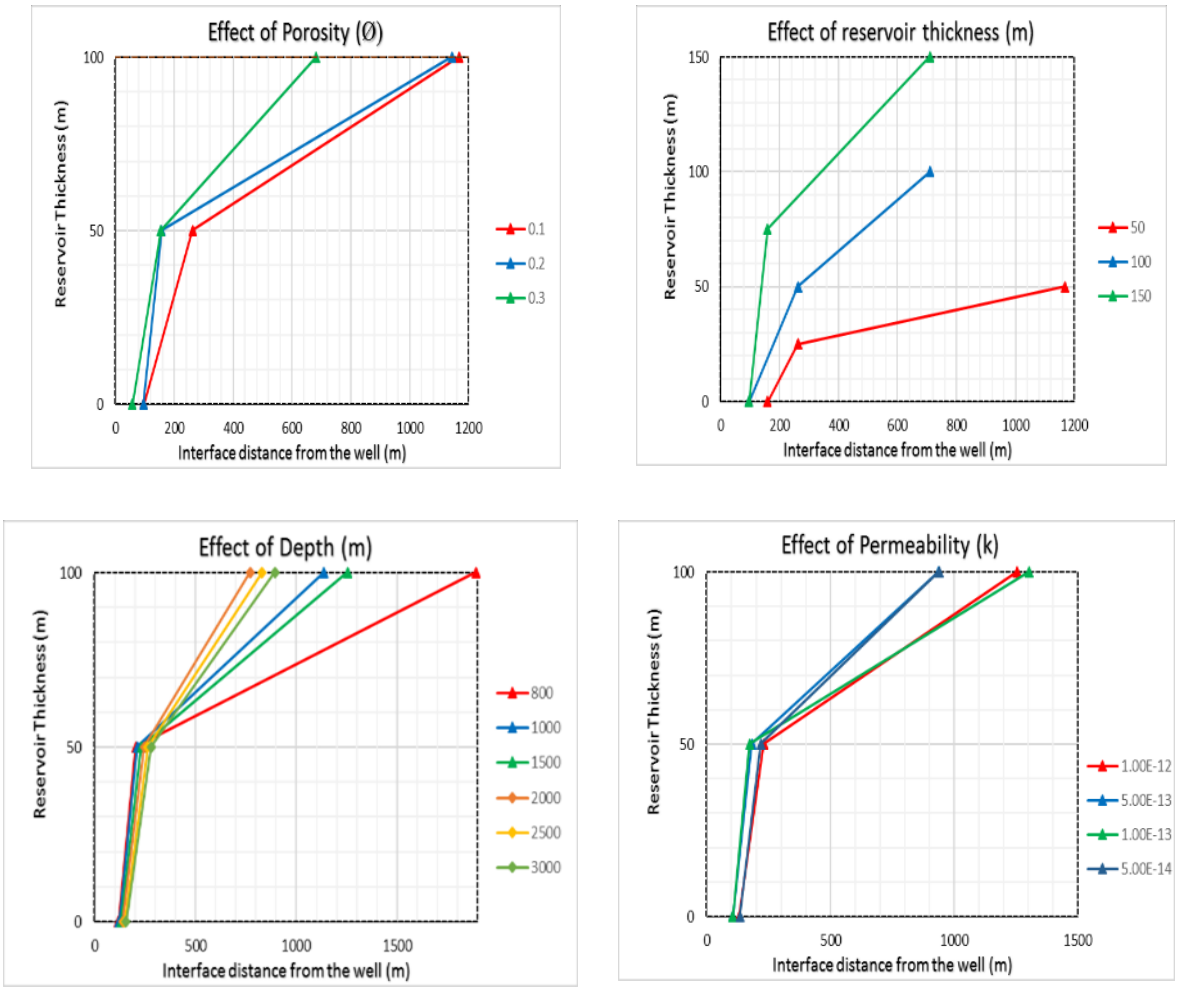

Figure 6: CO_2 / brine interface location as function of porous media reservoir parameters, for constant M_w = 100 kg/s, injection for 100 days, Brine density 1025 kg/m^3, well diameter 50 cm.

As for permeability, larger values lead to a larger plume at the middle extent of the plume, accordingly. The geothermal gradient has a direct effect on the top extent of the plume, with a higher geothermal gradient resulting in a thinner plume that extends further.

The middle extent of the plume is preferred as an indication of the thickness of the plume, while the top extent provides a better indication of the total distance covered by the plume at the top of the reservoir. A large top extent and small middle extent indicates a very thin plume accumulating at the top of the reservoir, a less interesting situation for CEEGS as the risk of producing brine would increase.

Figure 7 depicts tornado diagrams showing the sensitivity of the CO_2 plume interface to the range of parameters listed in Table 1. Obviously, the total injected mass of CO_2 is the most influential parameter for the size of the CO_2 plume, but since it is desirable to reduce the amount of time for the plume setup, the middle extent of the CO_2 plume is most sensitive to the porosity and the thickness of the reservoir. Both parameters are inversely correlated to the plume thickness, i.e. the plume thickness increases with decreasing porosity and thickness, which is not surprising since the same amount of CO_2 has less pore volume per unit bulk volume and needs to be accomodated further from the injection well. All other parameters are much less influential to the middle extent of the plume.

The top extent of the plume is more complex. The plume is still very sensitive and inversely correlated to the porosity and thickness, but reservoir depth is also a relevant influential factor, also inversely correlated to the plume extent due to the higher CO_2 density imposed by the increasing pressure. However, the plume extent is also very sensitive to increasing permeability and geothermal gradient, the former allowing higher transport distances and the latter implying lower CO_2 densities resulting, in both cases in larger, but thinner plumes.

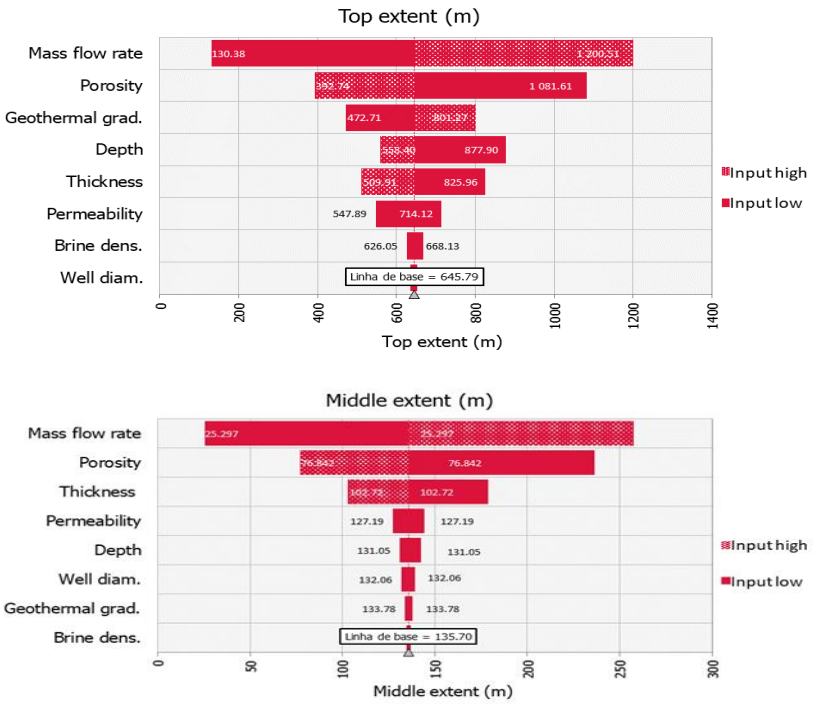

Figure 7: Sensitivity of the CO_2/brine interface location (middle extent and top extent) to porous media reservoir parameters.

Thus, the need to setup an initial CO_2 plume that is not too thin, implies that site screening for the CEEGS concept does not favour high porosity or very thick reservoirs, unlike in conventional CO_2 storage projects. Moreover, high permeabilities would result in plumes that cover a large area but that could be too thin to be of interest.

Figure 8 represents a cross plot by Hoffman et al. (2015) of thickness, permeability and injectivity[1] of the geological reservoirs in a number of important CO_2 storage projects worldwide. Hoffman et al. (2015) suggested a classification into three reservoir quality types. Type I covers thick reservoirs with injectivity above 100 darcy.metres and is represented by the well-known Sleipner and Snohvit CO_2 storage projects in the North Sea. Type II covers reservoirs with injectivity from 10 to 100 darcy.metres and is represented, for instance, by the Otway and Gorgon projects in Australia. Type III are lower permeability reservoirs, with injectivity below 10 darcy.metres, an example of which is the In Salah project in Algeria.

In type I reservoirs, a very thin plume results, such as is Sleipner. However, the CEEGS concepts favors thicker CO_2. This can be found in types II and III reservoirs, with lower permeability and less thick reservoirs. It is hypothesised that CEEGS should focus on geological settings in the range depicted by the dashed line polygon in Figure 8.

Hoffman et al (2015) do not include porosity in their cross plot, but in porous media reservoirs, there is some correlation between the effective porosity and the permeability, so that it could be considered that the polygon in Figure 9 also includes low to moderate porosities. The rule-of-thumb in CO_2 storage site screening process is to look for reservoirw with at least of 15% and as high as possible. For the CEEGS concept, it could be hypothesised that a porosity of 15% would not be a lower limit but could actually be the target value.

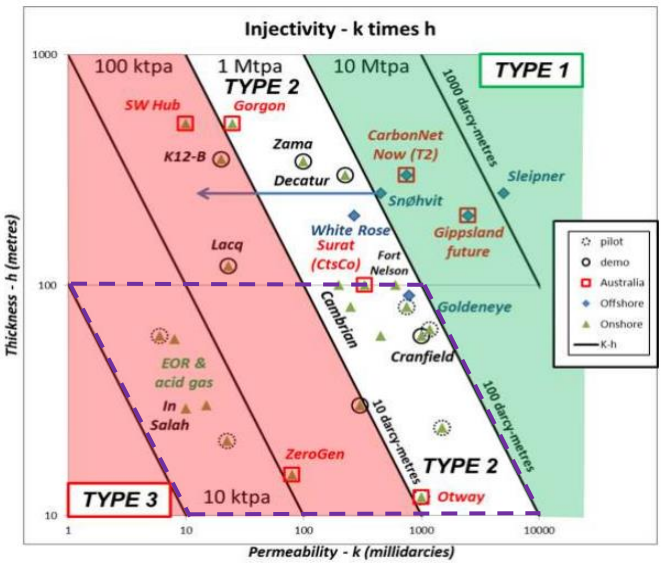

Figure 8: Thickness-Permeability cross plot for Injectivity (N.Hoffman et al., 2015))

[1] As is often the case in the CO_2 storage research community, Hoffman et al. (2015) designate the product of thickness and permeability by *Injectivity*, when in fact that product denotes transmissivity. For the sake of comparison with Hoffman et al. (2015) we will follow the same convention in this deliverable.

4.2 LIMITATIONS IMPOSED BY RESERVOIR DEPTH

Within the CEEGS concept, the efficiency of the system will depend partly on the underground component being able to deliver, at the wellhead of the back-production well, P-T values that are not much lower than those of the injection wellhead in the charge stage. Since pressure and temperature will vary in the wells due to gravitational and frictional losses, the depth of the reservoir will have a major impact on the P-T in the wellheads.

The wellbore model in section 3.3 allows for studying the influence of the reservoir depth to the P-T changes at the back-production well. Monte Carlo simulations were again used, with the set of parameters in Table 1, but considering now a discharge duration of 10 h. The reservoir pressure at the beginning of the cycle was calculated from the Mathias et al. (2009) solution (see section 3.1) for an injection well with a similar injection rate, and a maximum 20% gpressure build-up from the initial reservoir pressure. The reservoir temperature was considered in equilibrium with the geothermal gradient.

Figure 9 illustrates the pressure obtained in the wellhead of the back-production well in the discharge phase for different sets of reservoir depths. Table 2 shows the percentage of cases that resulted in CO_2 phase transitions within the well, as a function of reservoir depth and flow rate. Pressure losses in the back-production well can partially be managed by the well diameter and the well casing material (by decreasing the friction coefficient), but at an economic cost for large diameters at deep reservoirs.

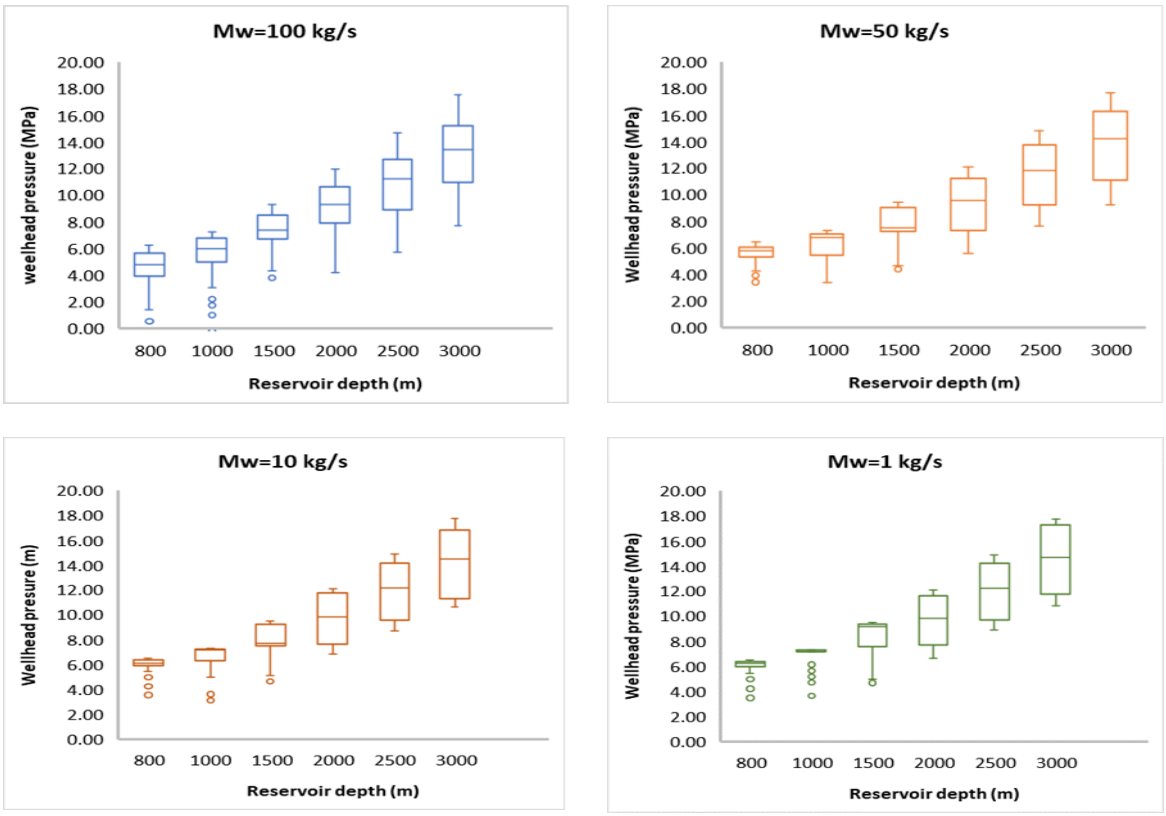

Figure 9: Expected wellhead pressures in the production well during the discharge phase as a function of reservoir depth, indicating when a phase transition occurs in the wellbore.

Since phase transitions in the well are undesirable due to sudden expansion of the fluid and due to wellhead pressures at the wellhead that are too low, Figure 9 and Table 2 show that CEEGS concept has little chances of being feasible for reservoirs shallower than 1000 m deep. As a rule-of-thumb, it is possible to say that the scenarios for CEEGS should consider:

- Reservoir depth of at least 1300m for mass flow rates up to 10kg/s (0.31MtCO_2/year). For comparison this would be CO_2 capture rate in a relatively small cement factory, and the admissible injection rate per well in a poor quality reservoir;
- Reservoir depth of at least 1500m for mass flow rates up to 50kg/s (about 1.57MtCO_2/year) and well diameter above 0.3m. This compares with a capture rate from a moderate size refinery or natural gas power plant, injecting at a single well in a good quality reservoir;

Reservoir depth of at least 1800m for mass flow rates of 100kg/s (about 3.15MtCO_2/year) and well diameter of 0.3m to 0.5m. This compares with a capture rate from a coal power plant or a large refinery, injecting at a single well in a very good quality reservoir.

Table 2: Percentage of cases with "in-well" phase transition

Depth (m)	Mw= 100 kg/s	Mw= 50 kg/s	Mw= 10 kg/s	Mw= 1 kg/s
800	100%	100%	100%	100%
1000	100%	100%	100%	100%
1500	49%	43%	15%	9%
2000	20%	27%	17%	20%
2500	5%	0%	0%	0%
3000	0%	0%	0%	0%

4.3 POROUS MEDIA, OPEN STRUCTURE

4.3.1 Charge stage

For the sake of simplicity, in the following discussion we are considering that the injection and bakcproduction facilities are composed by a doublet, i.e. by only two wells, A and B. Although such an arrangement is possible it is highly unlikely in the implementation of the CEEGS concept, which will probably required multiple injection and back-production wells. In a doublet arrangement, during the charge stage, well A is injecting at a constant rate to store CO_2 in the supercritical phase (Figure 10).

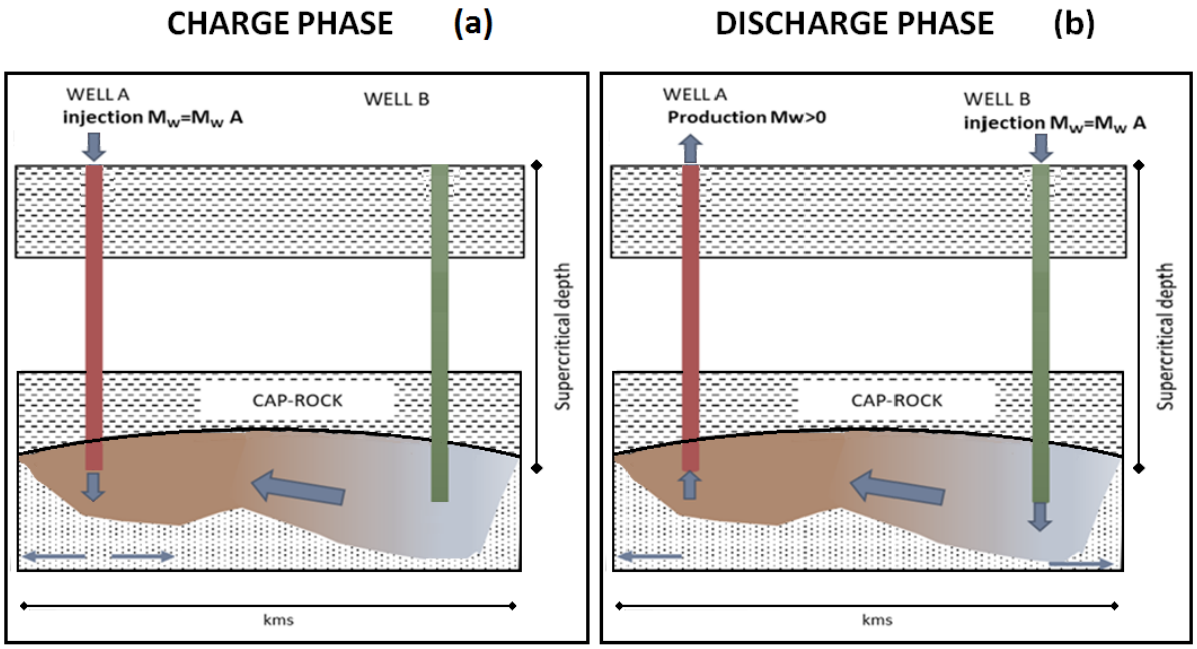

Figure 10: Schematic diagram of the charge (a) /discharge (b) cycle in an open structure in a porous media reservoir

In this stage, the major concerns for the underground component are the P-T conditions that should be delivered by the surface facilities to the injection wellhead A and the reservoir pressure build-up to avoid fracturing the reservoir or the cap-rock. Although at the detailed planning stage, geomechanical studies and definition of the existing stress-state are required to establish the maximum pressure build-up admissible in any reservoir, at early research stages it is common to admit a maximum percentual pressure build-up with respect to the initial reservoir pressure. It is common in CCS projects that the admissible pressure build-up varies between 10% to 20%, with the latter being assumed here.

Monte Carlo simulations were implemented with parameters in Table 1 to estimate the P-T conditions required at the well A during the charge stage.Figure 11 show sthe sensitivyt of the pressure buil-up solution to set of realistic parameters in Table 1. Although pressure build-up is primarily a function of the reservoir parameters (porosity, permeability, thickness, etc.), items such as mass flow rate and well diameter are managed by the operator and are of consequence for the pressure and temperature delivered by the surface components to the injection A wellhead. This pressure build-up can be computed from the reservoir solution of Mathias et al. (2009) given by equation 2, coupled with the wellbore model of Adams et al. (2014), equations 4 to 7.

An example is shown in Figure 12 for a mass flow rate of 16kg/s (0.5Mt/year), for a range of reservoir depths from 1500m to 3000m and for well diameters from 0.3m to 0.5m. The charge duration is 10 hours. The area between same colour solid and dashed lines indicates the range of wellhead P-T suitable for injection at different depths, with pressure build-up lower than 20% of the initial pressure, manageable through adoption of different well diameters. For a given wellhead pressure, higher wellhead temperatures will imply a lower CO_2 density, which will induce a lower bottomhole pressure that may not be sufficient to ensure injectivity. In that case higher wellhead pressures or smaller well diameters would be necessary.

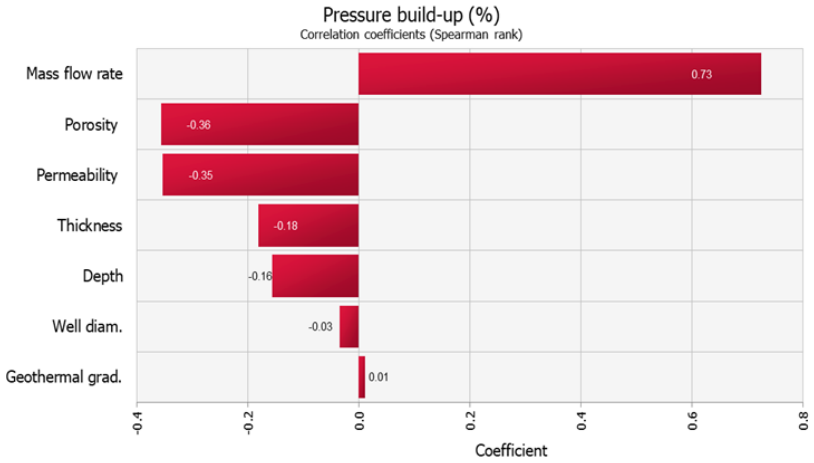

Figure 11: Sensitivity of pressure build-up to parameters in Table 1, as depicted by the correlation coefficient between the parameter values and the pressure build-up.

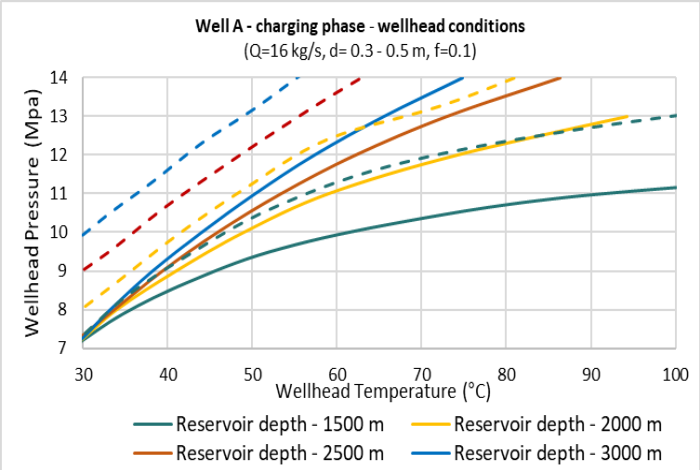

Figure 12: Wellhead P-T conditions for well A, charge stage. Q=16 kg/s, d= 0.3-0.5 m, f=0.1 at different depths (1500-300m).

Table 3 shows valid P-T conditions as a function of reservoir depth, injectivity (again defined as the product of thickness and permeability), geothermal gradient and mass flow rate, for a well diameter of 40 cm. The Monte Carlo realisations encompass wellhead P and T that range from 6MPa to 14MPa, in increments of 2MPa, and from 30°C to 110°C, in increments of 20°C [1]. The values not filled in the table do not allow for injection in the reservoir without inducing too high pressure build-up, at least with the 0.4 m diameter well.

[1] The sampling procedure in the Monte Carlo realisations utilise as input samples from the data set Table 1 with each value being equally likely, and P and T sampled from equally likely values from 6 MPa to 14 MPa, in increments of 2 MPa, and from 30ºC to 110ºC, in increments of 20ºC.

Obviously the mass flow rate and the reservoir depth (i.e, the initial reservoir pressure, since the pressure build-up is restricted to a maximum of 20% of the hydrostatic pressure) are the most relevant factors. The influence of injectivity becomes more noticeable for large mass flow rates, even for the wide range applied in this case (from 50 mD.m to 1000 mD.m), possibly due to the short duration of the charge stage.

The excel files that complement this report show the full range of simulations conducted and can provide insights for designing the surface facilities to deliver the required injection wellhead P-T conditions.

Table 3: Valid wellhead P-T conditions at injection well A, charge stage, for a well diameter of 0.4 m and for reservoir porosity of 10%.

Flowrate(kg/s)	Injectivity (x 1e-11)	Depth (m)														
		1000			1500			2000			2500			3000		
		Geothermal gradient (ºC/km)														
		20	30	40	20	30	40	20	30	40	20	30	40	20	30	40
10	0.5	10	10		10	10	10	14		14	14	14	14	12	12	12
		90	90		50	50	50	90		90	70	70	70	50	50	50
	1			10	10	10	10	14	14	14	14	14	14	12	12	14
				90	50	50	50	90	90	90	70	70	70	50	50	70
	5	8	8	8	12	12	12	12	12	12				14	14	14
		50	50	50	90	90	90	70	70	70				70	70	70
	10	8	8	8	12	12	12	12	12	12				14	14	14
		50	50	50	90	90	90	70	70	70				70	70	70
50	0.5													14		
														50		
	1				12			14	12	12	12	12	12	12		
					70			70	50	50	50	50	50	50		
	5			10	10	10	10	14	14		14	14	14	14	12	12
				70	50	50	50	90	90		70	70	70	70	50	50
	10				10	10	10	12	12	14			14	12	12	12
					50	50	50	70	70	90			70	50	50	50
100	0.5															
	1													14		
														50		
	5	10			10	12		14	14	12	12	12	12	12	12	12
		70			50	70		90	70	50	50	50	50	50	50	50
	10			10	10	10	10	14		14	14	14	14	12	12	12
				70	50	50	50	90		90	70	70	70	50	50	50

4.3.2 Discharge stage

In the discharge phase, both Well A and Well B are operational. Well A works as a production well, back-producing the CO_2 injected in the charge stage (Figure 10b). Well B, located at a distance from well A, here considered to be at the limit of the free-phase CO_2 plume created in the initial setup phase, reinjects the same mass flow of CO_2 produced in well A, but in liquid phase (see Figure 1:).

4.3.2.1 Production well A

Assuming that between the charge and discharge stages there is a similar time-period in which CO_2 is neither being injected and produced, it can be assumed that pressures in the reservoir equilibrated to the initial (before charge) pressures. Mathias et al. (2009) reservoir model and Adams et al. (2014) wellbore model can then be used to estimate the P-T conditions expected at the wellhead of well A, an essential input for the surface component of the discharge cycle.

Once again, the parameters in Table 1 were used to conduct Monte Carlo simulations for a set of realistic porous media parameters. Discharge periods of 10h were adopted. Figure 13 shows the pressure and temperature profile and the wellhead P-T conditions that would be obtained for reservoirs depths from 1800m to 3000m, and mass flow rate of 16kg/s and 100kg/s, in an 0.3m diameter well.

However, and although the pressures in the reservoir are likely to recover in the period between the charge and discharge period, the same is not likely to happen with the temperatures, since they will take more time to equilibrate. Thus, the downhole temperature estimated during the charge phase (see previous section) was used as the initial reservoir temperature in the discharge stage, well A. A further constraint was imposed that no-phase transition should occur within the well.

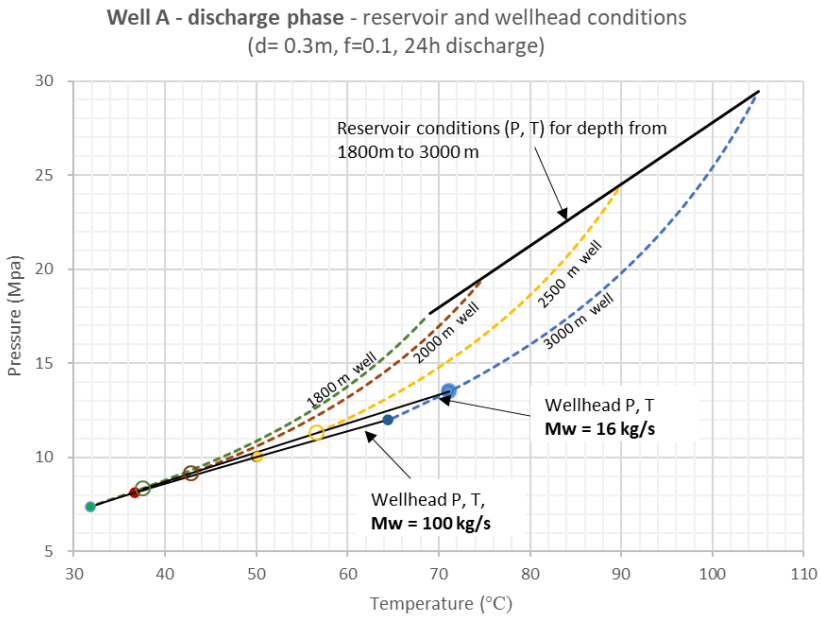

Figure 13: Pressure and temperature profiles in well A, back-producing CO_2 in the discharge phase, at mass rates of 16 kg/s (0.5 Mt/year) and 100 kg/s (3.1 Mt/year), assuming reservoir conditions before start of the discharge stage. Empty circles show P-T conditions at the wellhead for mass flow rate of 16 kg/s, filled circles show P-T conditions at wellhead for mass flow rate of 16 kg/s. Colours of circles are related to the depth of the aquifer as shown by the dashed lines.

Erro! Autorreferência de marcador inválida. shows a subset of the simulations implemented for this scenario, in this case for a well diameter of 0.4 m, and for a reservoir porosity of 10%. The complete

set of simulations are included in the excel files that are a supplement to this deliverable. **Erro! Autorreferência de marcador inválida.** shows the P-T conditions expected in the production wellhead A during the discharge stage, as a function of reservoir depth, geothermal gradient, mass flow rate and injectivity. The void cells denote cases in which either it was not feasible to inject such a mass flow rate in the charge stage without inducing non-admissible pressure build-up, or there was no viable solution to produce the CO_2, with that well diameter, without causing two-phase flow in the well itself. A decrease in the well flow rate or increase in the diameter would be necessary to make that scenario feasible.

Table 4: P-T conditions at wellhead A, for a diameter of 0.4 m. Discharge stage. Production well A. 10 hours discharge time.

Flowrate(Kg/s)	Injectivity (x 1e-11)	Depth (m)														
		1000			1500			2000			2500			3000		
		Geothermal gradient (ºC/km)														
		20	30	40	20	30	40	20	30	40	20	30	40	20	30	40
10	0.5	7	8		9	8	10	9	13	13	11	14	16	12	15	19
		27	32		34	36	53	37	59	75	49	72	100	57	87	124
	1	6	7	8	8	8	10	8	10	12	11	14	16	12	15	18
		21	31	34	32	36	52	34	52	74	48	71	99	56	87	123
	5	7	7	8	8	8	10	7	10	12	11	14	16	12	15	18
		27	31	34	34	36	52	32	50	74	49	72	100	57	87	123
	10	6	7	8	8	8	10	7	10	12	11	14	16	12	15	18
		21	31	34	32	36	52	32	48	73	48	71	99	56	87	123
50	0.5													15	18	
														65	93	
	1				7			9	11	14	11	13		13	18	20
					31			39	55	77	48	70		59	93	126
	5	7	7	8	7	8	10	8	11	14	11	14	16	12	15	18
		25	32	34	32	35	52	36	52	76	49	71	99	56	87	123
	10	7	7	8	7	8	10	7	10	12	11	13	16	12	15	18
		28	32	34	31	35	52	29	49	74	48	70	99	55	86	123
100	0.5															
	1													14	19	
														63	96	
	5	7			8	9	11	8	11	14	11	13	16	12	16	18
		27			33	38	55	34	55	77	47	70	98	57	87	122
	10	7	8	7	8	7	9	8	11	12	10	13	15	11	15	17
		28	32	31	31	31	50	32	54	72	46	69	98	53	84	121

4.3.2.2 Injection well B

The CEEGS discharge stage implies that CO_2 back-produced in well A, after expansion and cooled in a heat exchanger, must be injected at well B, most likely in a liquid state. The constraints to injection in well B are similar to those described in section 4.3.1 for well A, during the charge phase, when it is operating as an injection well, i.e., pressure build up below 20% of the initial pressure. The sensitivity of the downhole pressure to the wellbore and reservoir parameters are the same as described in section 4.3.1.

An example is show in Figure 14, for a mass flow rate of 16kg/s (0.5Mt/year), for a range of reservoir depths from 1500m to 3000m and for well diameters from 0.3m to 0.5m, for a discharge stage of 10 hours. The area between solid and dashed lines of the same colour indicates range of wellhead P-T suitable for the injection at different depths with pressure build-up lower than 20% of the initial pressure, manageable through adoption of different well diameters.

Given that the density of the liquid phase of CO_2 is much higher than that of the supercritical phase, downhole pressures in the injection well B will be higher than those imposed downhole well A when injecting supercritical CO_2 (see Figure 12), thus requiring lower wellhead pressures in well B than in well A.

Monte Carlo simulation were conducted for different geothermal gradients, depths, injectivities, diameters and flowrates for wellhead pressure 5.5 MPa and well temperature 10°C. The results are included in the excel data file that are a part of this deliverable.

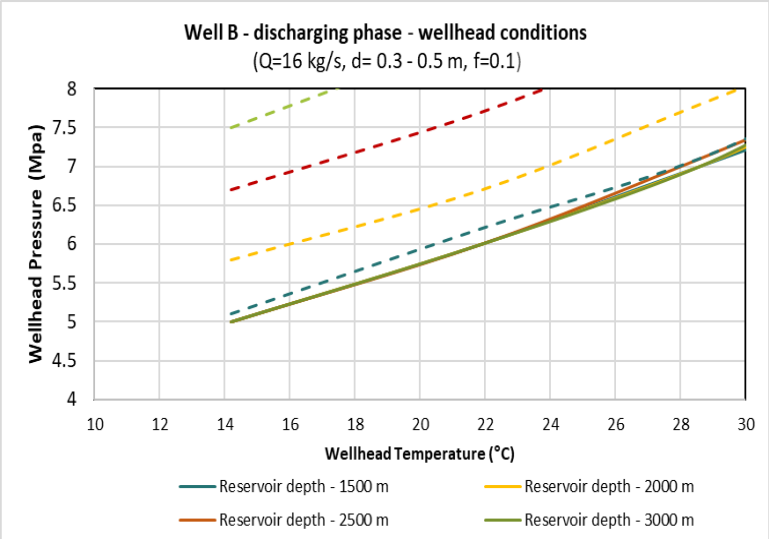

Figure 14: P-T wellhead conditions during discharge stage required for CO_2 injection in well B, at different depths. Charge phase. Q=16 kg/s, d= 0.3 - 0.5 m, f=0.1

4.4 POROUS MEDIA, CLOSED STRUCTURE

The porous media scenario described in the previous section refers to an open structure in which there are no lateral impermeable boundaries preventing the migration of brine away from the injection well under the influence of a hydraulic gradient. In such a structure, CO_2 is stored in the pore space by pushing away the brine. However, it is possible to envisage the implementation of the CEEGS concept

in closed structures, i.e. in porous reservoirs bounded by impermeable boundaries, such as impermeable faults or pinch-outs (Figure 15). This kind of structural trap is very common both for deep saline aquifers and depleted hydrocarbon fields. In such structures, the CO_2 is stored due to the compressibility of rock, water and CO_2, and not by the availability of pore space (although the buoyancy effect will lead to the CO_2 accumulating on the top of the structure).

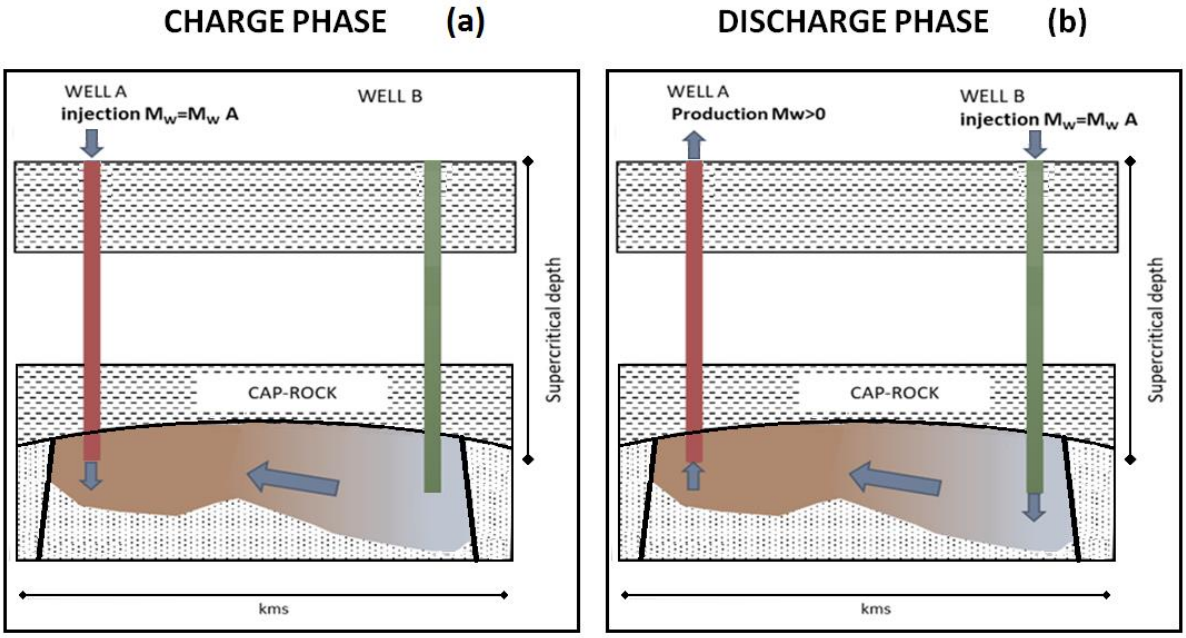

Figure 15: Schematic diagram of the charge (a) /discharge (b) cycle in an open structure in a porous media reservoir.

In a closed structure, all CO_2 and brine are trapped structurally with no lateral flow. This has advantages and disadvantages for the CEEGS concept. Given that the storage efficiency factor is much lower than for open structures, the same mass of CO_2 will occupy a much larger volume. That is, a large CO_2 plume can be setup in less time and with less mass of CO_2.

In a closed structure, pressure will not entirely dissipate when the injection is stopped (or at least not at the same rate as in an open structure). Only with the progress of dissolution and mineral trapping do pressures start decreasing noticeably. The initial plume setup will lead to a meaningful pressure increase in the structure (see for instance Bergmo et al. (2011) solution in equation 3).

Referring to the analysis conducted about the reservoir depth limitations in section 4.1, higher reservoir pressures will allow to decrease the reservoir depth necessary to ensure that no phase transition occurs in the well. Given that we are adopting a maximum pressure increase of 20% of the initial pressure, the required depth of the reservoir would decrease by roughly the same proportion: for instance, the 1200 m depth can probably be relaxed to around 950 m deep in closed structures (Table 5). While there is no valid solution for an open structure for a reservoir at 1000 m deep, the closed structure allows to obtain supercritical CO_2 at the wellhead of the producing well.

A further advantage is that the higher reservoir pressures allow to obtain higher P-T values in the producing wellhead A during the discharge phase, as depicted for a few sample cases in Table 5, obtained through coupling of the reservoir model, the wellbore flow and the pressure increment estimated by the equation 3 for a closed structure.

Table 5: Comparison between PT wellhead for open and closed aquifer during discharge phase (flowrate 10kg/s, D=0.3m, H = 100m, k= 500 md, geothermal gradient = 30 °C/km and discharge time = 24h).

	Closed Aquifer		Open Aquifer	
Depth (m)	**Wellhead P (Mpa)**	**Wellhead T (ºC)**	**Wellhead P (Mpa)**	**Wellhead T (ºC)**
1000	6.43	25.04	-	-
1500	7.62	32.87	7.58	32.75
2000	10.57	51.92	9.86	48.95
2500	12.67	67.93	12.26	66.61

However, it is this same non-dissipation of the pressures that lies at the root of the main disadvantages of the closed boundaries scenario. The pressure build-up will increase much faster in this structure, thus the mass flow rate of CO_2 in each cycle, or the duration of the cycle, will have to decrease in order to respect the maximum pressure build-up of 20%.

Another important disadvantage is that, while in open structures the brine migrates away from the injection well, leaving only a residual water saturation, in closed stuctures all the brine remains in the structure, increasing the possibility of producing brine during the discharge phase, either directly or due to dissolution from supercritical CO_2. in fact, if the porous media is a depleted hydrocarbon field, the higher mobility of hydrocarbons due to contact with CO_2 will lead to its production during the discharge phase.

These interactions are not possible to understand clearly with analytical solutions and will be studied in detail with numerical models in task 2.2.

4.5 TWO AQUIFERS AT DIFFERENT DEPTHS

While the previous scenarios targets one single deep reservoir, it is possible to envisage the implementation of the CEEGS concept with two porous media reservoirs at different depths. A similar concept of energy storage was first suggested by Liu et al. (2016), although not including thermal energy storage at the surface, only compressing and expansion cycles, much like in CAES.

In Liu et al. (2016) setup the first reservoir is a low-pressure reservoir used to store CO_2 exhausted from the turbine, whereas the second reservoir is at higher pressure to store CO_2 from the compressor (Figure 16). According to the authors, the system could be operated in two different ways with regard to the state of CO_2:

i. by allowing the CO_2 to transition from supercritical to gaseous conditions in the turbine;
ii. by keeping the CO_2 in supercritical phase throughout the cycle.

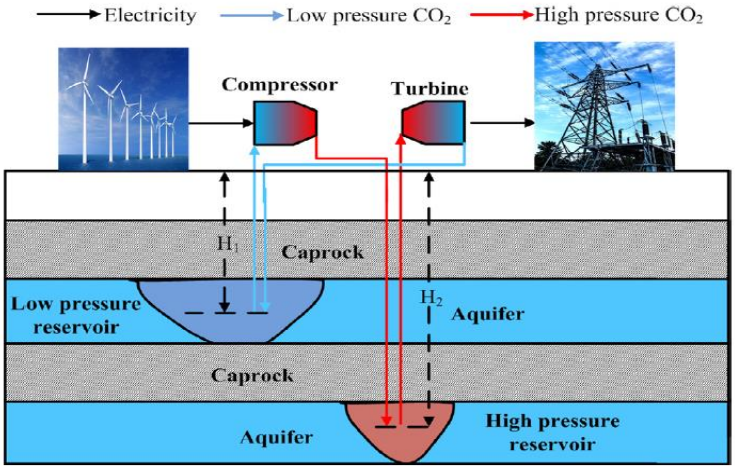

Figure 16: Schematic illustration of in Liu et al. (2016) energy storage system using two saline aquifer reservoirs.

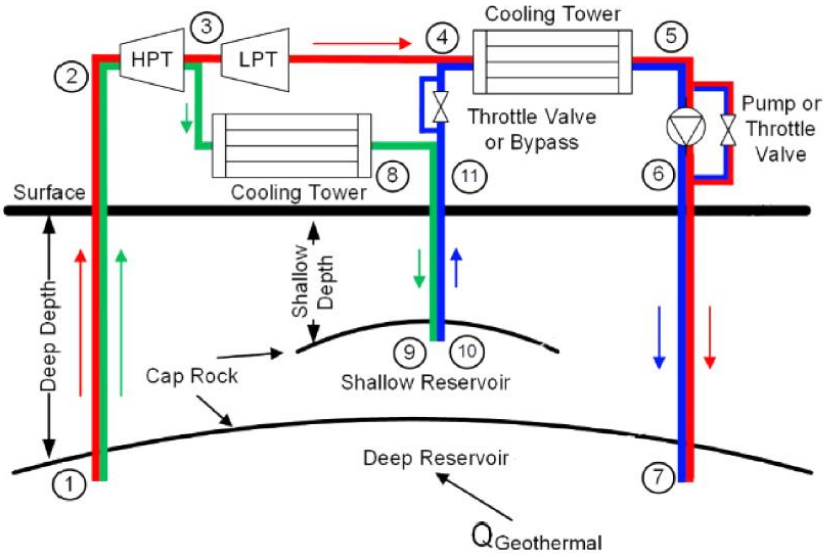

Figure 17: System diagram for a "CO_2-plume geothermal" facility operating to provide dispatchable power (red lines), energy storage (blue lines for power consumption; green lines for power generation), and both services simultaneously (red + green + blue lines) (Fleming et al., 2022).

Simulations performed by Liu et al. (2016) indicated that the system has a larger energy storage density (497.68 k h/m^3 for transcritical CO_2 and 255.20 kWh/m^3 for supercritical CO_2) compared to CAES (2–20 kW h/m^3) and a round-trip efficiency (63.35% for transcritical CO_2 and 62.28% for supercritical CO_2). It is also noted that the low-pressure reservoir needs to be much shallower and larger than the supercritical CO_2 energy storage reservoir. Therefore, it may pose higher environmental risks.

A related concept was introduced by Fleming et al. (2022) and Van Brummen et al. (2022), in both cases referring essentially to a deep geothermal system using CO_2 as the working fluid, and resorting to a shallower aquifer for temporary storage of CO_2 when there is not demand for energy production from the geothermal system (Figure 17).

Both system described above are inherently simpler than the CEEGS concept, since they lack the surface thermal energy storage system implemented at surface, with Liu et al. (2016) relying on mechanical (pressure) energy storage in depth, and the Van Brummen et al. (2022) and Fleming et al. (2022) being essentially a CO_2-enhanced geothermal system with intermediate storage of CO_2.

Nevertheless, the studies conducted by those authors demonstrate that two porous media reservoirs at different depths can provide a viable scenario for implementing the CEEGS concept:

- During the charge stage, the CO_2 is produced in gas or supercritical phase from a shallower reservoir, through well B. It is compressed and transfers heat to the hot storage at surface, after which it is injected through well A in supercritical phase in a deep reservoir;
- In the discharge stage, CO_2 is produced at high pressure at well A, recovers heat from the hot storage, generates electricity through expansion in a turbine and is cooled in a heat exchanger, before being reinjected into the shallower reservoir through well B at gas or supercritical phase.

The difference between the scenarios with a single reservoir and this scenario is that CO_2 is kept circulating in both reservoirs during the charge and discharge phases. Also, an initial setup phase is required in both reservoirs instead of being only implemented through well A. Due to CO_2 lateral migration, dissolution and residual trapping in both aquifers, a permanent source of CO_2 will still be required. Since there is no possibility of migration between the shallow and deep reservoirs, as they are separated by one or several cap-rocks, there is no geothermal heat gain during the discharge cycle. That would only be possible for very long cycles that allow for the CO_2 in the deeper reservoir to equilibrate with the reservoir temperature, possibly for seasonal storage.

Storage in gas phase will require aquifers shallower than 700 m and with a large pore volume, so that the plume may become very large, imposing a higher risk of leakage into shallower groundwater systems.

No simulations were conducted for this scenario, since the analytical solutions would not retrieve meaningful differences from the simulations for the single porous media reservoir, but task 2.2 will implement the two-aquifers case in the numerical modelling studies.

5 SALT CAVITIES SCENARIOS

While in porous media the flow rate and the pressure variations are dictated by the reservoir petrophysical parameters, such as permeability, porosity and rock compressibility, in salt cavities higher storage pressures are admissible and P-T variations can be better managed.

5.1 SALT DISSOLUTION CAVITY

This scenario mimics the natural gas and compressed air energy storage systems (CAES). In conventional Diabatic CAES, surplus renewable energy is utilised to compress air, with resulting heat being wasted to the atmosphere, and inject it in a salt dissolution cavity through a well. When there is demand, the air is back-produced through the same well, heated by natural gas, and expanded in a turbine connected to a generator, so that energy is restored. In Adiabatic CAES, which is at a much lower TRL, the heat generated in the compression stage is stored (much like in CEEGS) and recovered during the expansion stage, avoiding the need to heat the air with natural gas.

This scenario utilises essentially the same principle, with one salt dissolution cavity being used to store CO_2 during the charge stage, and CO_2 being back-produced from the same cavity in the discharge stage, using one sigle injection/ production well. However, unlike in CAES, CO_2 cannot be released to the air, implying that a surface storage (tank) of CO_2 is required during the discharge stage.

5.1.1 Admissible cavity depths

Experimental investigations on rock salt cores under pressurisation with supercritical CO_2 proved that a pressure-driven opening of grain boundaries in polycrystalline rock salt and, thus, a loss of tightness only occurs when the CO_2 pressure significantly exceeds the minimum principal stress (Minkley et al. 2022). This means that the maximum storage pressure is limited by the minimum principal stress in the salt rock acting in the cavern roof, i.e. by lithostatic pressure (Soubeyran et al., 2019). Therefore, pressures admissible in salt caverns are considerably higher than those admissible in porous media, which are a function of hydrostatic pressure and are often limited to 20% of pressure build-up.

We followed the maximum and minimum values pressures often used as pressure limits in the CAES industry and defined by Allen et al. (1982) (and also followed by Soubeyran et al. (2019)) as :

1. Maximum pressure P_{max} = 0.8 lithostatic pressures
2. Minimum pressure P_{min} = 0.3 lithostatic pressures and above 7.4 MPa (to ensure supercritical CO_2). This minimum pressure is required to avoid closure of the cavity and is maintained by the cushion gas.

Figure 18 shows a calculation of the admissible working pressure and temperature expected in salt cavity for different geothermal gradients and considering a lithostatic pressure calculated (in MPa) as P=0.022z (Soubeyran et al., 2019), where z is the depth of the top of the salt cavity.

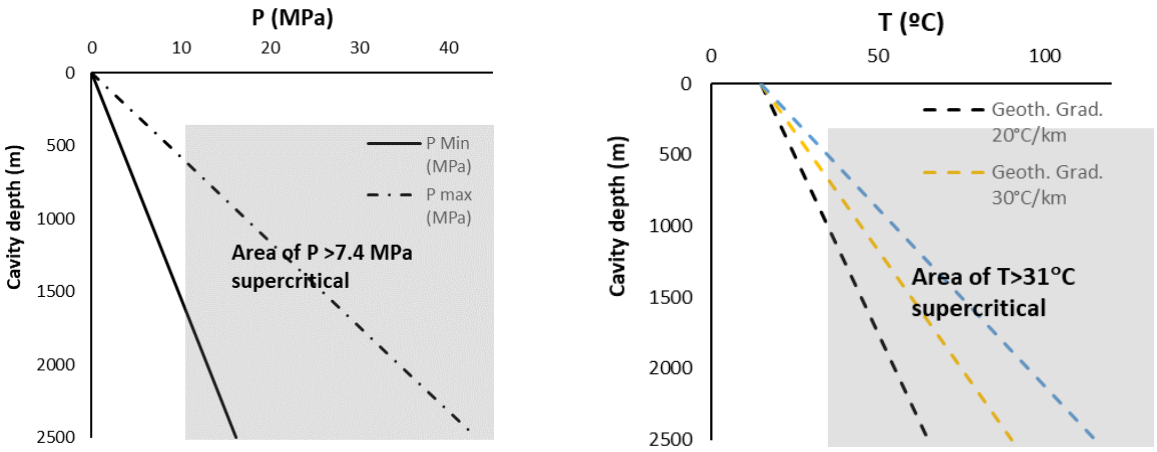

Figure 18: Expected P and T at the top of the cavity with respect to depth

To ensure supercritical CO_2 behaviour, considering the pressure and temperature gradients in Figure 18 and operating the cavity near the minimum pressure imposed by the cushion gas, the minimum salt cavity depth required would be 1200 m, while the maximum salt cavity depth would be the same as usually recommended for CAES or natural gas storage, 2500 m to avoid salt plasticity at high temperatures (Allen and Doherty, 1982).

If a decision is made to operate the cavities near the maximum allowed pressure, then under normal geothermal gradient conditions, the minimum required depth for the top of salt cavity would be 550 m. This situation would be possible, if the CEEGS charge/discharge cycles impose the circulation of only a small percentage of the stored CO_2, which could often be the case for storage cycles of a few hours.

Salt cavities have also been studied as a possibility for permanent CO_2 sequestration (Dusseault et al., 2013; Zhang et al., 2022), but this scenario has a limited potential in that respect. For instance, as shown in Figure 19, even for large cavities with a total volume of 500 000 m^3, the amount of CO_2 that can be stored at high depth is relatively small (350-400 kton). Still, it is comparatively much higher that the CO_2 mobilised in hourly cycles, and a management decision of maximising the CO_2 sequestered in the long term may lead to operate the cavity near its maximum allowed pressure, in which case the admissible salt cavity depth could be in the order of the 500-600 m, while maintaining supercritical behaviour.

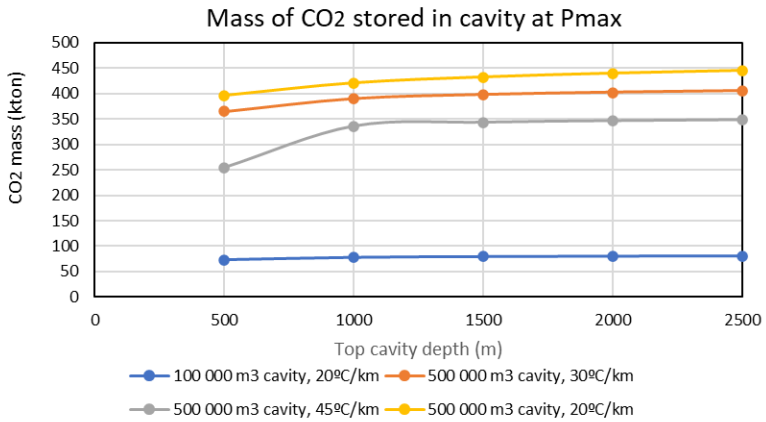

Figure 19: Mass of CO_2 stored in cavity at the maximum admissible pressure.

5.1.2 Surface storage requirement

Unlike the CAES analogue scenario, CO_2 must be stored at the surface in the discharge stage, when backproduced from the well and before being reinjected in the cavity in the next charge cycle. This naturally imposes constraints on the cycles' duration and the mass flow rates in the charge/discharge cycles, since the size (and cost) of the surface tanks will become an important variable.

Table 6 includes a crude estimate of the volume of CO_2 circulated in 5h and 10h cycles and for mass flow rates of 100kg/s and 500kg/s. The range of circulated CO_2 mass is compatible with surface tanks and moreover, shows that the percentage of circulated CO_2 is a minor fraction of the total CO_2 stored in salt cavities. The cavities would then be managed (from the point of view of pressures) near the maximum admissible pressure, allowing for shallower caverns and maximising the CO_2 indefinitely sequestered in the cavity.

Table 6: Surface tank volume for storage in the liquid phase

Flow rate (kg/s)	Cycle duration (h)	CO_2 circulated volume per cycle (m^3) *
100	5	2 075
100	10	4 150
500	5	10 373
500	10	20 747

* For surface storage conditions at P= 5 MPa and T=10°C, at liquid CO2 density of 867 kg/m3.

5.1.3 Expected wellhead conditions

Whether for the porous media scenarios or the salt cavity scenarios, the most relevant parameters related to the underground component are the pressure and temperature conditions, both at the charge stage (well operating as injection) or the discharge stage (well back-producing CO_2).

Using the salt cavity model (equation 8), and the wellbore flow model (equations 4 to 7), the average P-T in the salt cavity and the pressure loss in the back-production wellbore can be estimated. Figure 20 shows the average evolution of P and T in a very large salt cavity (1 million m^3), with the top located at 800 m depth, in which the CO_2 is injected at a rate of 200 kg/s, in 5 h cycles of charge and discharge, with a wellhead injection pressure of 7.5 Mpa and temperature of 45°C.

It is not aimed here to characterise extensively what those P-T conditions might be under different salt cavity storage scenarios. Nevertheless, a few examples cases are indicated to provide an order of the P-T conditions that might be expected at the wellhead in the discharge stage and required at the wellhead for injection given the pressure in the salt cavity. The cases tested are characterised in Table 7.

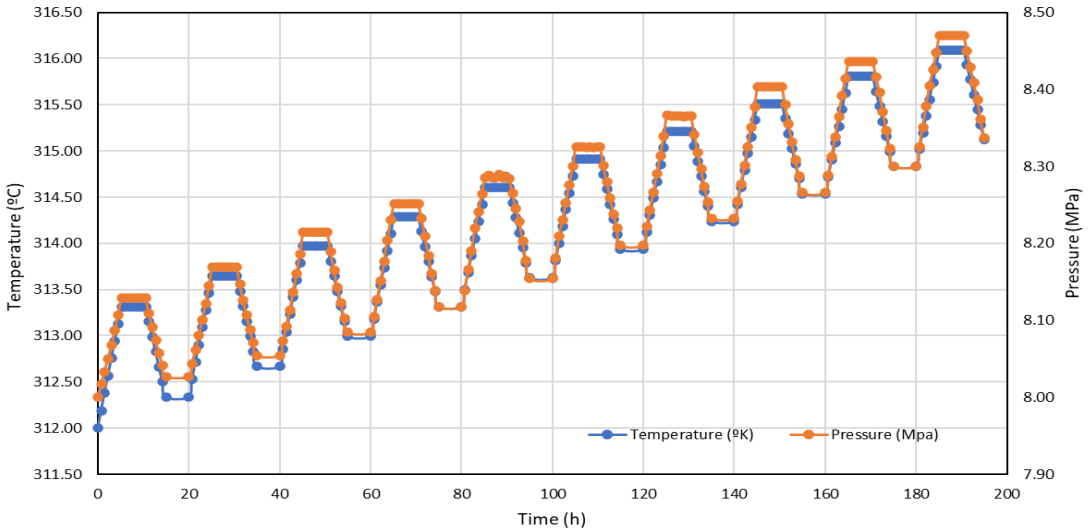

Figure 20: Average pressure and temperature in salt cavity during the charge/discharge cycle**.**

Table 7: Single cavity test cases

Cavity volume (m3)	33510	(equivalent to 20 m radius spherical cavity	
Depth (m)	500	1000	1500
Maximum Pressure (MPa)	8.63	17.27	25.9
Minimum Pressure	3.23	6.48	9.71
Initial cavity temperature (ºC)	30	45	60
Wellhead Injection pressure (MPa)	5	7	8
Wellhead Injection Temperature (MPa)	30	35	40
Mass flow rate (kg/s)	100		
Well diameter (cm)	50		
Cycle duration (h)	5		

The average P and T in the salt cavity for 20 charge / discharge cycles were estimated and are depicted in Figure 21, while the pressure drop in the back-production well is show in Figure 22.

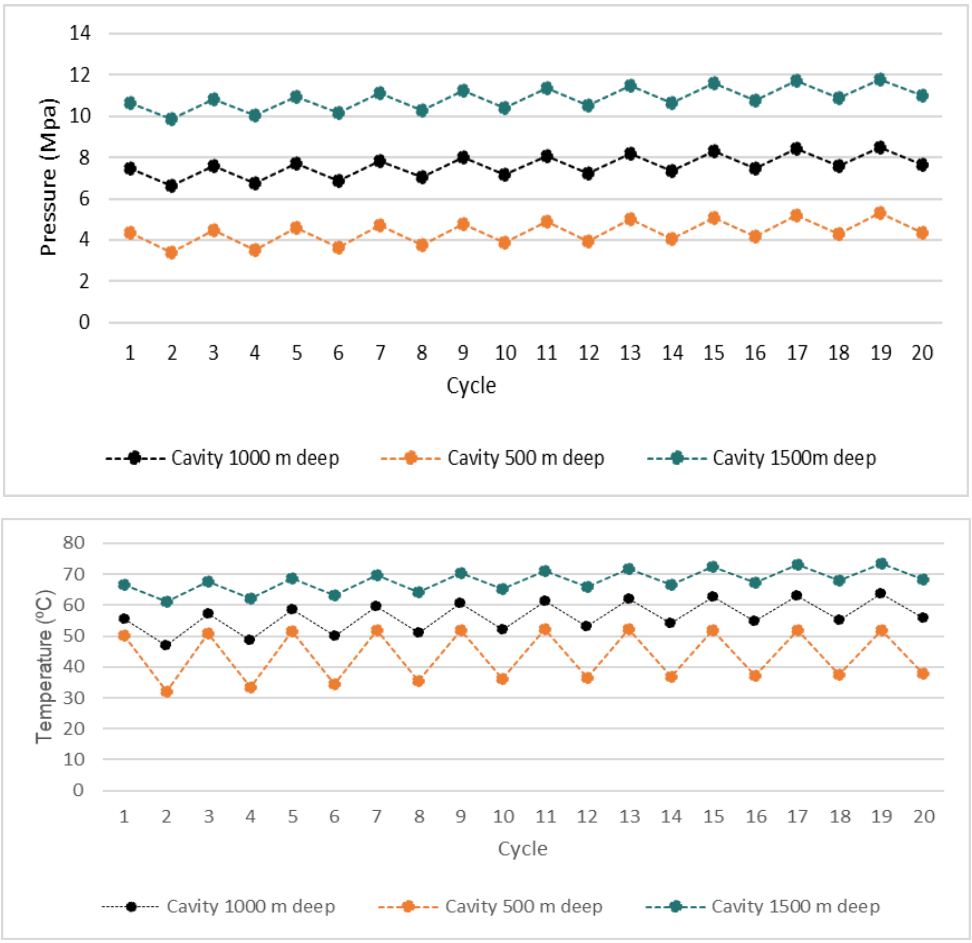

Figure 21: Variation of average pressure and temperature in salt cavity during the charge/discharge cycle. Only the P and T at the end of charge/discharge cycle (dots) are results from the model, dotted lines are illustrative, do not show the evolution of P and T within each cycle

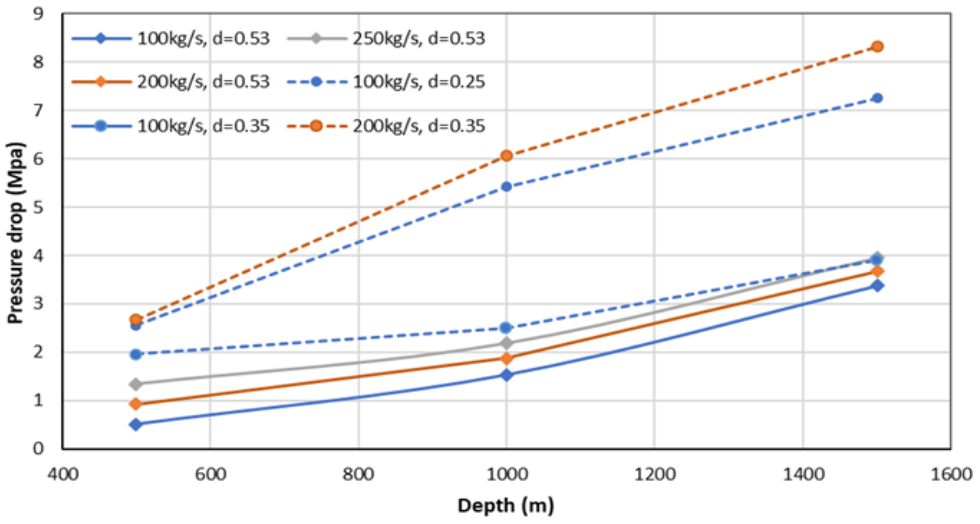

Figure 22: Pressure drop in the back-production wellhead at the end of the 1st discharge cycle for several well diameters and mass flow rates.

5.2 TWO SALT DISSOLUTION CAVITIES

The possibility of utilising two salt cavities for energy storage with supercritical CO_2 as the working fluid was recently suggested by Minkley et al. (2022). The concept is based on two caverns in rock salt, in which supercritical CO_2 is stored under different pressure and temperature conditions (Figure 23).

According to the calculations of those authors, utilising a high-pressure cavern (0.8 million m^3) at 1500m depth and a low-pressure cavern (1 million m^3) at 800m depth, connected through wells and pipes 20" (50.8cm) diameter, at a mass flow rate of **1200 kg/s** a peak power of 9 MW could be obtained. The gravity-induced pressure drop alone is about 12 MPa, and the friction-induced pressure drop is 2 MPa, resulting in an inlet pressure at the turbine that is reduced by about 14 MPa. During the storage cycles, a CO_2 mass exchange of less than 5% takes place between the caverns. The efficiency was calculated at about 50%.

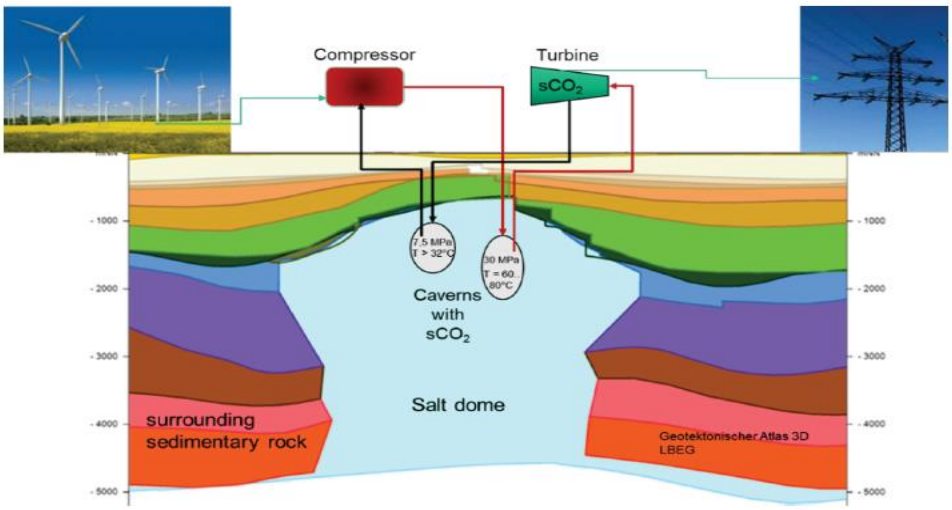

Figure 23: Basic principle for a cavern storage power plant in a salt dome with high-pressure and low-pressure cavern and sCO_2 turbine and compressor at the surface (Minkley et al., 2022).

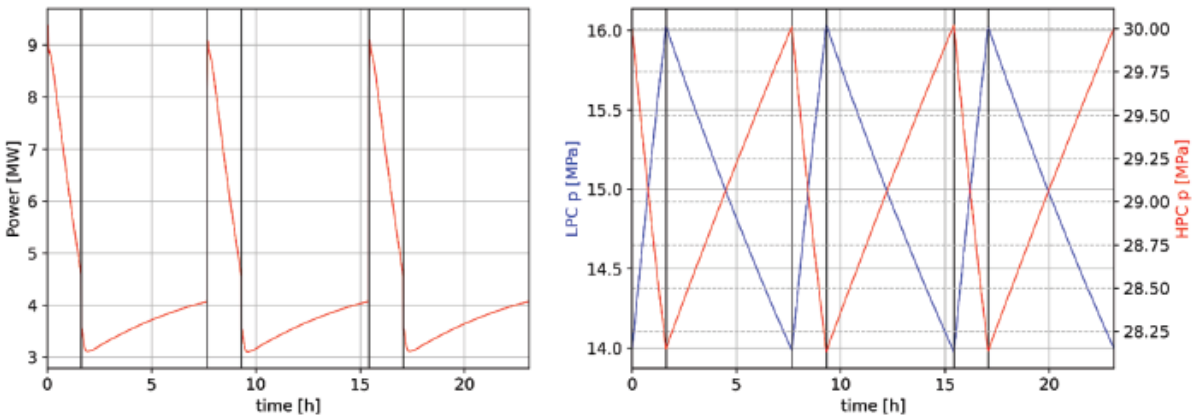

Figure 24: Calculated power for 3 storage cycles in salt caverns with supercritical CO_2 turbine and compressor at the surface connected by 20" tubing (left). Cyclic pressure changes in caverns (right): (Minkley et al., 2022).

The main difference between Minkley et al. (2022) concept and the CEEGS concept is that no thermal heat storage occurs in the surface, with the energy storage being mostly in the mechanic (pressure) form, much like in the CAES.

However, the energy storage capacity estimated by Minkley et al. (2022) using two cavities is very interesting and can be adapted to the CEEGS concept. The advantage of this scenario is that, unlike the scenario with a single cavity, it allows to utilise much larger mass flow rates (because it does not require surface tanks), and it allows for a large pressure difference between the two cavities.

It is possible to envisage that during the discharge cycle, the CO_2 could be stored in the low-pressure cavity in the supercritical or *gas* phase, the latter allowing for shallower cavities. The possibility of CO_2 being stored in a gas phase in the discharge cycle also opens up the possibility of utilising decommissioned salt mines, usually with very large volumes, or brine production mines, as low-pressure cavities.

In the charge cycle, the CO_2 would have to be stored in the supercritical state, requiring depths of at least 550 m when operating close to the maximum admissible pressures, or 1200 m when pressure management is closer to the minimum admissible pressures.

5.2.1 Expected wellhead conditions

To test the expected wellhead conditions when using two salt cavities, several scenarios were analysed with the salt cavity thermodynamic model in equation 8 and the wellbore model in equations 4 to 7.

5.2.1.1 Cavities at same depth - pressure managementI

Considering two salt cavities at the same depth with the overall properties and parameters (Table 8) based on the Huntorf CAES facilities. During the charge cycle, with a surplus of renewable energy, CO_2 is injected in the high-pressure cavity in supercritical phase up to a maximum pressure of 11.4 MPa, while during the discharge cycle, CO_2 is back-produced from that cavity and injected in the low-pressure cavity, at a similar depth but operating near the lower pressure limit of 4.2 MPa, thus being in a gas phase.

Figure 25 and Figure 26 represent the pressure variation expected in the high-pressure cavity, and in the low-pressure cavity, in orange and blue lines respectively, while the dots represent the wellhead pressures, for 20 charge / discharge cycles.

Table 8: Salt cavities parameters used for scenario based on Huntorf cavities (Raju and Kumar Khaitan, 2012)

	High pressure cavity	Low Pressure cavity
Volume	140 000	170 000
Depth	650	600
P Max (Mpa)	11.2	11.2
P Min (Mpa)	4.2	4.2
Cavern Temperature	34.5	24
Well diameter (cm)	53.34	53.34
Charge / discharge time (h)	5	5
Mass flow rate (kg/s)	**100**	**100**

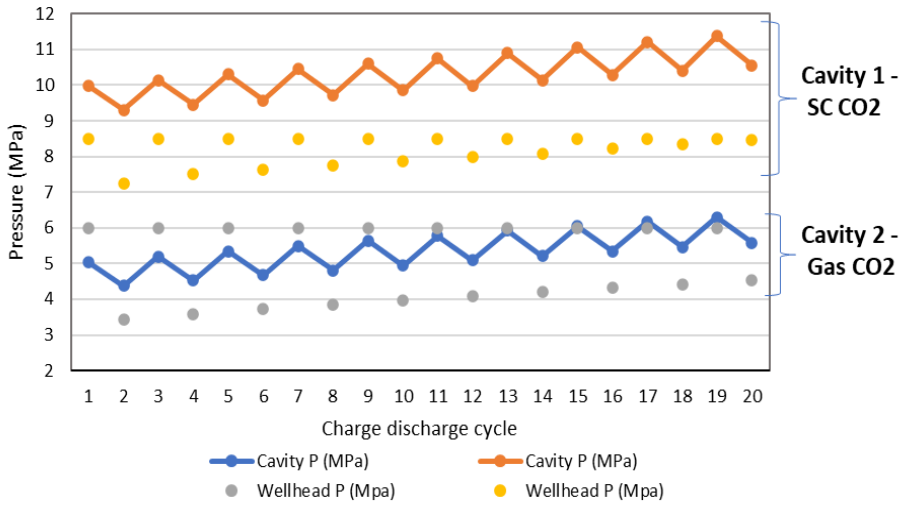

Figure 25: Pressure variation in the two salt cavities (high and low pressure). Lines are the pressure variation in the two cavities. Dots are wellhead pressure during the charge/discharge cycles.

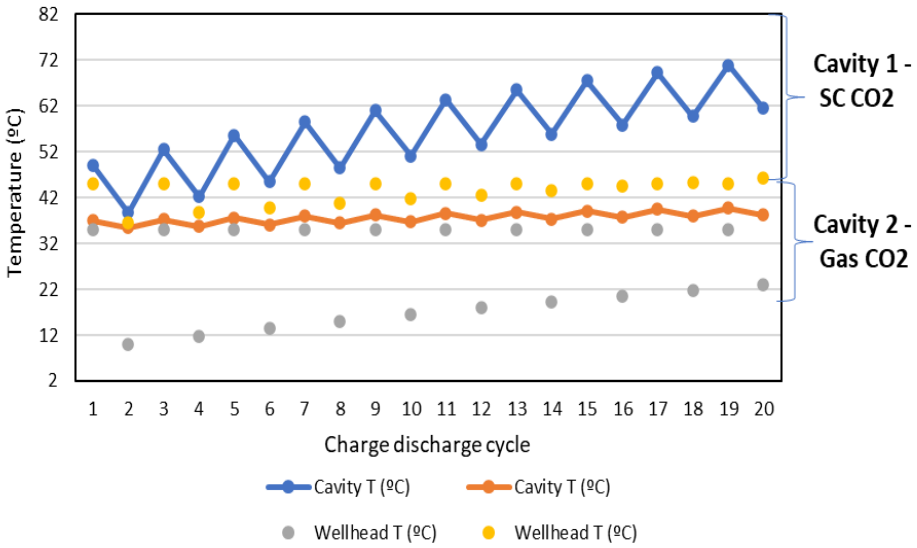

Figure 26: Temperature variation in the two salt cavities (high and low pressure). Lines are the temperature variation in the two cavities. Dots are wellhead temperatures during the charge/discharge cycles.

5.2.1.2 Cavities at different depths

A second scenario considered is taken from Minkley et al. (2022), utilising large salt cavities (0.8 and 1 million m^3) at very different depths (800m and 1500 m), with a considerable gap in the admissible pressure differences (Table 9). Figure 27 and Figure 28 represent the pressure variation between the two cavities. The percentage of CO_2 circulated between the cavities in each charge / discharge cycle is relatively small, 9% of the CO_2 stored in the high pressure cavity.

Table 9: High and pressure salt cavities parameters used for the calculation.

	Scenario Minkley et al. (2022) - HP and LP salt cavities	
	HP Cavity	LP Cavity
Volume	800 000	1 000 000
Depth	1500	800
P Max (Mpa)	25.90	13.81
P Min (Mpa)	9.71	5.18
Cavern Temperature	60	39
Well diameter (cm)	50.8	50.8
Discharge period (h)	5	5
Mass flow rate (kg/s)	**200**	**200**
% circulated	**9%**	

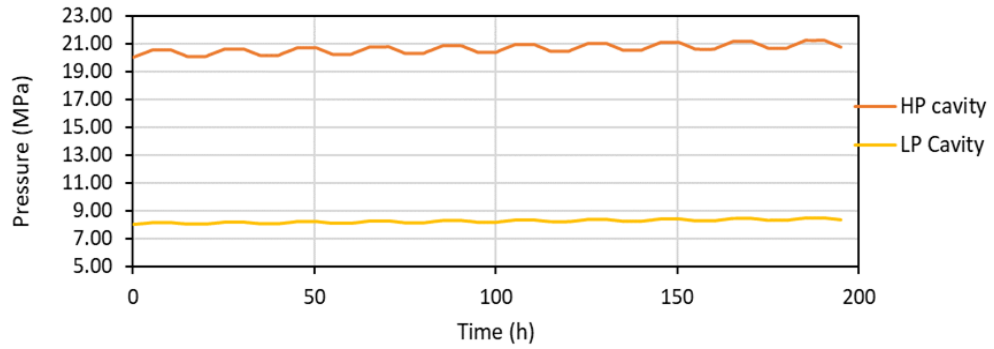

Figure 27: Pressure variation with time in the two salt cavities (high and low pressure).

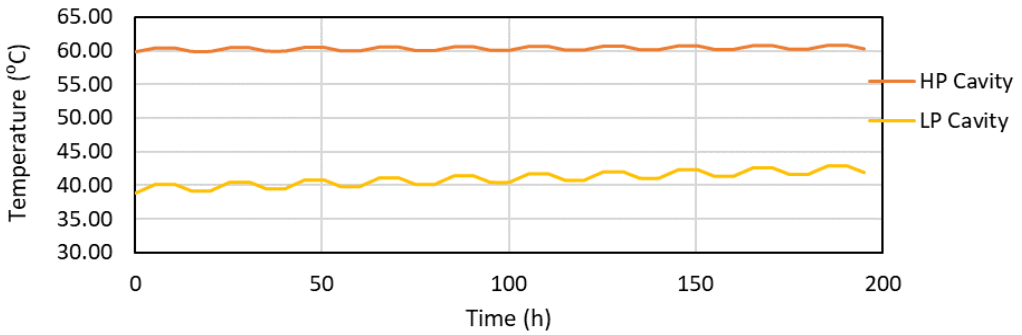

Figure 28: Temperature variation with time in the two salt cavities (high and low pressure).

6 KEY COMPONENTS OF SCENARIOS FOR NUMERICAL MODELS

Given the results in the previous chapters, the geological scenarios to be considered in subsequent tasks of WP2 and, if proved valid, in other work packages, include the following (Table 10):

i. Porous media reservoirs: deep saline aquifer (DSA) with an open structure.
ii. Porous media reservoirs: DSA with a closed structure.
iii. Porous media reservoirs: depleted hydrocarbon field (closed structure)
iv. Porous media reservoirs: Two DSAs at different depth)
v. Geothermal sedimentary system
vi. Salt layers: One salt dissolution cavity and surface tank
vii. Salt layers: Two salt dissolution cavities.

Notice that geothermal sedimentary were nowhee specifically addressed in this deliverable, but that geothermal gradient was considered a variable in every Monte Carlo realization conducted in chapters 3 and 4. Temperature in the reservoir, porous media or salt cavity, was always considered a linear function of the geothermal gradient, and the sensitivity analysis proved that the geothermal gradient does have play an important role to the setup stage (section 4.1), to the selection of the reservoir (section 4.2) or cavity depth (section 5.1.1) and to the expected wellheads pressures and temperature at the back-production well (section 4.3.2.1).

Each scenario will be characterised by ranges of hydraulic and thermodynamic conditions, using simplifying assumptions about the geometry of the reservoirs, and whenever possible, using real data (Table 10). It is not implied that the scenarios are all feasible for CEEGS, since the analysis made using the analytical solutions in chapter 2 are simplifications of a complex problem. It is likely that detailed modelling will result in dropping some of the scenarios, for instance due to the quality of the CO_2 that can be produced.

In fact task 2.2 will devleop numerical models to consider the transient behaviour of pressure and temperature variation during the charging/discharging cycles and represent the influence of the geological setting on the overall efficiency of the system. The simulations will consider the transient behaviour and pressure-depressurization cycles, and the reservoir cooling induced by the charging-discharge cycles. Task 2.3 upscales the analysis to clarify the development of CO_2 trapping mechanisms in the subsurface, and the changes to the fluid composition that will result from the reaction of the CO_2 with the reservoir minerals and brine, as well as from the pressure and temperature varying conditions.

Still the approach will be inherently different for porous media resrevoirs and salt cavities. The approach for porous media implementing numerical models that will try to reproduce actual field conditions, and will not attempt to connect to the surface facilities (something to be done at later WPs). The salt cavities approach, because of the lesser number of variables, will focus on integrating the solutions presented in this deliverable together with the thermodynamic models that describe the surface components of the CEEGS concept.

Table 10 list the essential data that will integrate the scenarios, not only for WP2, but also for other WPs, such as for instance the geomechanical parameters, since the geomechanical behaviour is beyond the goals of WP2.

Table 10: Key components of scenarios to study with numerical approach

Geological Environment	Deep saline aquifer (open and closed)	Two deep saline aquifers	Depleted hydrocarbon field	Geothermal	Salt Cavities (one and two cavities	Source of Data
RESERVOIR DEFINITION						
Open structure geometry	**X**		**X**	**X**		Simplified real data
Closed structure geometry	**X**	**X**				Simplified real data
Heterogeneity	**X**	**X**	**X**			Simplified real data
CHEMICAL PARAMETERS						
Reservoir lithology (detailed mineralogy)	**Siliciclastic**	**Siliciclastic**	**Siliciclastic**	**Sedimentary system (Carbonate)**		Real data
						Real data
Formation water chemical composition	**X**	**X**	**X**	**X**		Real data
Residual water saturation	**X**	**X**	**X**	**X**		Literature
Residual hydrocarbons composition			**X**			Real data
Capillary pressures	**X**	**X**	**X**	**X**		Literature
Reactive surface area or grain radius	**X**	**X**	**X**	**X**		Literature
PETROPHYSICAL PARAMETERS						
Permeability	**10 - 1000 mD**	**10 - 1000 mD**	**10 - 1000 mD**	**10 - 1000 mD**		
Relative permeabilities	**X**	**X**	**X**	**X**		Literature
Porosity	**0.1 - 0.20**	**0.1 - 0.20**	**0.1 - 0.20**	**0.01 - 0.05**		
THERMAL PARAMETERS						
Geothermal gradient	**20 - 40°C/km**	**20 - 40°C/km**	**20 - 40°C/km**	**40 - 60°C/km**	**20 - 40°C/km**	
Rock thermal conductivity	**X**	**X**	**X**	**X**	**X**	Literature
Rock thermal capacity	**X**	**X**	**X**	**X**	**X**	Literature
GEOMECHANIC PARAMETERS						
Rock compressibility	**X**	**X**	**X**	**X**	**X**	Literature
Elastoplastic parameters reservoir	**X**	**X**	**X**	**X**	**X**	Literature
Elastoplastic parameters cap-rock	**X**	**X**	**X**	**X**	**X**	Literature

7 CONCLUSIONS

This study investigated different geological conditions in which CEEGS technology could effectively store energy and promote subsurface CO_2 sequestration. An analytical and semi-analytical modelling approach has been implemented to investigate the favourable geological condition for different proposed geological environments. For given geological conditions, sensitivity analyibsis based on Monte Carlo realisations were conducted to understand subsurface constraints and Pressure and Temperature conditions in the reservoir and between wellheads and bottomhole during charge-discharge cycles.

The analytical and semi-analytical solutions allow to analyze the constraints that reservoir depth, petrophysical parameters and hydraulic conditions may impose to the implementation of the CEEGS concept in these environments. This approach was applied to: i) porous media, either deep saline aquifers or depleted hydrocarbon fields; ii) salt cavities. The overall goal of the deliverable was to provide a first identification of the likely scenarios in which the CEEGS concept can potentially be applied and the constraints imposed by those geological environments to its implementation.

The study encompassed both open and porous media reservoirs, and included the possibility of simultaneous utilization of two porous media reservoirs at different depths. It is recommended that site selection for porous media reservoirs, put less weigth on finding high permeability-high porosity, very thick reservoirs (type I reservoirs), as is often the case in the CO_2 storage technology, and is suggested that lower quality (type II and III) thinner reservoirs may present more favourable conditions for CEEGS. It is also recommended that the minimum reservoir depth to be deeper than in the CO_2 storage industry, at least 1300 m, to avoid CO_2 in-well phase transition.

Salt cavities scenarios were addressed for scenarios involving a single cavity coupled with surface CO_2 storage in a tank, but also in two salt cavities at different depths (or managed at different pressures). The range of admissible depths for the cavities and the expected wellhead pressures that can be obtained were studied for simplified cases.

The report concludes by listing the realistic geological scenarios that should be studied using numerical models in subsequent tasks of WP2, and if proved valid, in other WPs. The scenarios include various configurations of deep saline aquifers (open structure, closed structure, two aquifers), depleted hydrocarbon fields (closed structure), geothermal sedimentary system, and salt cavities (one single cavity with surface storage of CO_2, and two salt cavities). The numerical modelling studies will address the transient behaviour of the reservoirs, to understand the cyclic and long term evolution of pressure and temperature in the reservoir and wellheads, and chemical changes that may occur during the injection and back-prodution cycles due to the interaction between the CO_2 and the brine and mineral components of the reservoir.

These are key issues to clarify the feasibility of CEEGS in the proposed geological environments and they will be addressed in task 2.2 - *CO_2 Injection/production cycles* - and task 2.3 - *CO_2 sequestration and CO2 stream geochemical changes.*

REFERENCES

Adams, B.M., Kuehn, T.H., Bielicki, J.M., Randolph, J.B., Saar, M.O., 2014. On the importance of the thermosiphon effect in CPG (CO 2 plume geothermal) power systems. Energy 69, 409–418. https://doi.org/10.1016/j.energy.2014.03.032

Allen, R.D., Doherty, T.J., Thoms, R.L., 1982. Geotechnical factors and guidelines for storage of compressed air in solution-mined salt cavities. Pacific Northwest Lab., Richland, WA (USA).

Atrens, A.D., Gurgenci, H., Rudolph, V., 2010. Electricity generation using a carbon-dioxide thermosiphon. Geothermics 39, 161–169.

Atrens, A.D., Gurgenci, H., Rudolph, V., 2009. CO2 thermosiphon for competitive geothermal power generation. Energy & fuels 23, 553–557.

Bachu, S., 2003, Screening and ranking of sedimentary basins for sequestration of CO2 in geological media in response to climate change: Environmental Geology, v. 44, no. 3, p. 277-289.

Bachu, S., 2008, CO2 storage in geological media: role, means, status and barriers to deployment: Progress in Energy and Combustion Science, v. 34, no. 2, p. 254-273.

Bergmo, P. E. S., Grimstad, A.-A., and Lindeberg, E., 2011, Simultaneous CO2 injection and water production to optimise aquifer storage capacity: International Journal of Greenhouse Gas Control, v. 5, no. 3, p. 555-564.

Buckley, S.E., Leverett, M.C., 1941. Mechanism of Fluid Displacement in Sands.

Cornet, J.S., Dabrowski, M., Schmid, D.W., 2018. Long term creep closure of salt cavities. Int. J. Rock Mech. Min. Sci. 103, 96–106.

Dentz, M., Tartakovsky, D.M., 2009. Abrupt-Interface Solution for Carbon Dioxide Injection into Porous Media 15–27. https://doi.org/10.1007/s11242-008-9268-y

Dusseault, M. B., Rothenburg, L., and Bachu, S., 2013, Sequestration of CO₂ in Salt Caverns, Canadian International Petroleum Conference.

Fleming, M. R., Adams, B. M., Ogland-Hand, J. D., Bielicki, J. M., Kuehn, T. H., and Saar, M. O., 2022, Flexible CO2-plume geothermal (CPG-F): Using geologically stored CO2 to provide dispatchable power and energy storage: Energy Conversion and Management, v. 253.

Hou, Z., 2003. Mechanical and hydraulic behavior of rock salt in the excavation disturbed zone around underground facilities. Int. J. Rock Mech. Min. Sci. 40, 725–738.

Khaledi, K., Mahmoudi, E., Datcheva, M., Schanz, T., 2016. Analysis of compressed air storage caverns in rock salt considering thermo-mechanical cyclic loading. Environ. Earth Sci. 75, 1–17. https://doi.org/10.1007/s12665-016-5970-1

Kushnir.R, Ullmann, A., Dayan, A., 2012. Thermodynamic Models for the Temperature and Pressure Variations Within Adiabatic Caverns of Compressed Air Energy Storage Plants. https://doi.org/10.1115/1.4005659

Liu, H., He, Q., Borgia, A., Pan, L., and Oldenburg, C. M., 2016, Thermodynamic analysis of a compressed carbon dioxide energy storage system using two saline aquifers at different depths as storage reservoirs: Energy Conversion and Management, v. 127, p. 149-159.

Mathias, S.A., González, G.J., Miguel, M. De, Thatcher, K.E., Zimmerman, R.W., 2011. Pressure Buildup During CO 2 Injection into a Closed Brine Aquifer 383–397. https://doi.org/10.1007/s11242-011-9776-z

Mathias, S.A., Hardisty, P.E., Trudell, M.R., Zimmerman, R.W., 2009. Approximate solutions for pressure buildup during CO2 injection in brine aquifers. Transp. Porous Media 79, 265–284. https://doi.org/10.1007/s11242-008-9316-7

Metz, B., Davidson, O., de Coninck, H. C., Loos, M., and Meyer, L. A., 2005, IPCC Special Report on Carbon Dioxide Capture and Storage Cambridge University Press, 442 p.:

Minkley, W., Brandt, M., Dostál, V., Stepanek, J., Lehman, J., 2022. Energy storage in salt caverns with supercritical CO2, in: The Mechanical Behavior of Salt X: Proceedings of the 10th Conference on the Mechanical Behavior of Salt (SaltMech X), Utrecht, The Netherlands, 06-08 July 2022. CRC Press, pp. 639–651.

Minkley, W., Mühlbauer, J., 2017. Constitutive models to describe the mechanical behavior of salt rocks and the imbedded weakness planes, in: The Mechanical Behavior of Salt–Understanding of THMC Processes in Salt. CRC Press, pp. 119–127.

NETL, 2013, Site Screening, Selection, and Initial Characterisation for Storage of CO2 in Deep Geologic Formations. 2013 Revised Edition: National Energy Technology Laboratory, DOE/NETL-2013/1605.

N.Hoffman, Carman, G., Bagheri, M., Goebel, T., 2015. Site characterisation for carbon sequestration in the near shore Gippsland Basin. pp. 1–41.

Nordbotten, J.M., Celia, M.A., 2006. An improved analytical solution for interface upconing around a well. Water Resour. Res. 42, 1–10. https://doi.org/10.1029/2005WR004738

Oldenburg, C. M., 2008, Screening and ranking framework for geologic CO2 storage site selection on the basis of health, safety, and environmental risk: Environmental Geology, v. 54, no. 8, p. 1687-1694.

Pan, L., Freifeld, B., Doughty, C., Zakem, S., Sheu, M., Cutright, B., Terrall, T., 2015. Fully coupled wellbore-reservoir modeling of geothermal heat extraction using CO2 as the working fluid. Geothermics 53, 100–113.

Pan, L., Oldenburg, C.M., 2013. T2Well—an integrated wellbore–reservoir simulator. Comput. Geosci. 65, 46–55.

Pan, L., Webb, S.W., Oldenburg, C.M., 2011. Analytical solution for two-phase flow in a wellbore using the drift-flux model. Adv. Water Resour. 34, 1656–1665.

Pola, K., 2021. Influence of the Variability of Compressed Air Temperature on Selected Parameters of the Deformation-Stress State of the Rock Mass Around a CAES Salt Cavern.

Pruess, K., 2006. Enhanced geothermal systems (EGS) using CO2 as working fluid—A novel approach for generating renewable energy with simultaneous sequestration of carbon. Geothermics 35, 351–367.

Pruess, K., 2005. ECO2N: A TOUGH2 fluid property module for mixtures of water, NaCl, and CO2. Lawrence Berkeley National Laboratory Berkeley, CA.

Pruess, K., Garc, J., 2002. Multiphase flow dynamics during CO 2 disposal into saline aquifers 282–295.

https://doi.org/10.1007/s00254-001-0498-3

Raju, M., Khaitan, S.K., 2012. Modeling and simulation of compressed air storage in caverns: a case study of the Huntorf plant. Appl. Energy 89, 474–481.

RIAZ, A., HESS, H.A.T., ORR, F.., 2006. Onset of convection in a gravitationally unstable diffusive boundary layer in porous media. J.Fluid Mech 548, 87–111. https://doi.org/10.1017/S0022112005007494

Soubeyran, A., Rouabhi, A., and Coquelet, C., 2019, Thermodynamic analysis of carbon dioxide storage in salt caverns to improve the Power-to-Gas process: Applied Energy, v. 242, p. 1090-1107.

Van Brummen, A. C., Adams, B. M., Wu, R., Ogland-Hand, J. D., and Saar, M. O., 2022, Using CO2-Plume geothermal (CPG) energy technologies to support wind and solar power in renewable-heavy electricity systems: Renewable and Sustainable Energy Transition, v. 2.

Xia, C., Zhou, Y., Zhou, S., Zhang, P., Wang, F., 2015. A simplified and unified analytical solution for temperature and pressure variations in compressed air energy storage caverns. Renew. Energy 74, 718–726.

Yale, D. P., Nabor, G. W., Russell, J. A., Pham, H. D., and Yousef, M., 1993, Application of Variable Formation Compressibility for Improved Reservoir Analysis, 68th Annual Technical Conference and Exhibition of the Society of Petroleum Engineers: Houston, Texas, Society of Petroleum Engineers, Inc. , p. 435-450.

Zhang, Q.Y., Duan, K., Jiao, Y.Y., Xiang, W., 2017. Physical model test and numerical simulation for the stability analysis of deep gas storage cavern group located in bedded rock salt formation. Int. J. Rock Mech. Min. Sci. 94, 43–54.